# UNRAVELING CRP/cAMP-MEDIATED METABOLIC REGULATION IN *ESCHERICHIA COLI* PERSISTER CELLS

Han G. Ngo[1], Sayed Golam Mohiuddin[1], Aina Ananda[2], Mehmet A. Orman[1,*]
[1]Department of Chemical and Biomolecular Engineering, University of Houston, TX, 77204
[2]Department of Biology, Monmouth University, NJ, 07764
[*]Corresponding author: morman@central.uh.edu

## ABSTRACT

A substantial gap persists in our comprehension of how bacterial metabolism undergoes rewiring during the transition to a persistent state. Also, it remains unclear which metabolic mechanisms become indispensable for persister cell survival. To address these questions, we directed our efforts towards persister cells in *Escherichia coli* that emerge during the late stationary phase. These cells have been recognized for their exceptional resilience and are commonly believed to be in a dormant state. Our results demonstrate that the global metabolic regulator Crp/cAMP redirects the metabolism of these antibiotic-tolerant cells from anabolism to oxidative phosphorylation. Although our data indicates that persisters exhibit a reduced metabolic rate compared to rapidly growing exponential-phase cells, their survival still relies on energy metabolism. Extensive genomic-level analyses of metabolomics, proteomics, and single-gene deletions consistently emphasize the critical role of energy metabolism, specifically the tricarboxylic acid (TCA) cycle, electron transport chain (ETC), and ATP synthase, in sustaining the viability of persisters. Altogether, this study provides much-needed clarification regarding the role of energy metabolism in antibiotic tolerance and highlights the importance of using a multipronged approach at the genomic level to obtain a broader picture of the metabolic state of persister cells.

## INTRODUCTION

Bacterial persisters within cell cultures constitute a small subpopulation of cells exhibiting a transient antibiotic-tolerant state [1]. While persisters have traditionally been characterized as non-growing and dormant phenotypes [2], recent studies challenge these conventional hallmarks, revealing the heterogeneity of persister cells in terms of growth, metabolism, and other cellular activities [3–11]. Despite potential discrepancies in research outcomes in the field, we think that these variations arise from the intricate and diverse survival mechanisms employed by bacterial cells in response to adverse conditions, such as antibiotic treatments. Furthermore, the interplay of stochastic and deterministic factors associated with these mechanisms adds another layer of complexity, with outcomes highly contingent on factors such as cell types, antibiotics, and experimental and growth conditions [12]. The persistence phenomenon presents a significant health concern [13,14], as the transient antibiotic-tolerant state of persister cells promotes recurrent infections [15] and establishes them as a reservoir for the emergence of antibiotic-resistant mutants [16–18].

Drug tolerance is a widespread phenomenon observed in both prokaryotic and eukaryotic cell types. Otto Warburg's research in the early twentieth century unveiled an intriguing aspect of mammalian cell metabolism known as "aerobic glycolysis," wherein proliferating cells (e.g., tumor cells) derive energy predominantly through glycolysis, even in the presence of oxygen [19]. This metabolic reprogramming involves restricting entry into the TCA cycle through precise enzymatic control, diverting glycolytic intermediates towards anabolic pathways. This adaptation supports the extensive biosynthesis required for active cell proliferation in tumors [20]. Remarkably, tumorigenic persisters that exist in a non-proliferating state may not primarily depend on aerobic glycolysis. Instead, there is substantial evidence suggesting that these cells rely on energy metabolism [21,22]; however, the presence of this metabolic state in antibiotic-tolerant bacteria is still a question mark [10]. Reprogramming energy metabolism seems to be an evolutionarily conserved strategy for cells facing stress or adverse conditions, as these cells might benefit from the significantly higher ATP production efficiency provided by oxidative phosphorylation [20]. The identification of a mechanism shared by diverse cell types could open avenues for the development of global strategies to target drug-tolerant cells effectively.

A recent study suggests that bacterial persisters constitute a stochastically formed subpopulation of low-energy cells, despite some observed overlap in ATP levels between antibiotic-sensitive and persister cells [23]. The persister cells examined in that study were derived from an aged stationary phase culture (48 hours post-inoculation) [23], a condition known to elevate the number of non-growing cells, which do not promptly resume growth upon transfer to a fresh medium [24]. While the non-growing cells formed during the stationary phase have reduced metabolic activity compared to growing cells, as demonstrated in our earlier study [11], they still exhibit a certain degree of respiratory activity when their metabolism was characterized within the stationary phase culture [10]. We found that although there were significantly more persister cells in this non-growing cell subset, persister cells were still present in the growing cell populations [11]. This finding also aligns with another independent study, which utilized single-cell analysis, reporting that ofloxacin persisters were metabolically active cells in exponentially growing cultures before treatment and these cultures were obtained from 16-hour overnight precultures (not aged) [25]. The nature of persister-cell metabolism in bacteria is a topic that has long been a point of contention in scientific circles. The controversy surrounding this topic primarily arises from studies that rely on bacteriostatic chemicals or a limited number of gene deletions, or direct comparisons to exponentially growing cells, all of which have inherent drawbacks [10,11,23,26]. The metabolism of persister cells, a very complex phenomenon, cannot be easily characterized by a simplistic term such as “metabolic dormancy”. Even if persister cells may exhibit a lower metabolism compared to the vast majority of rapidly growing exponential-phase cells, they may still rely on energy metabolism for their functioning [27,28]. In fact, analyzing published studies collectively suggests that bacterial cell metabolism undergoes intricate alterations or rewiring as they transition into a tolerant state, and these alterations seem to be highly dependent on the specific conditions tested [3–7,9–11].

To gain a better understanding of the critical role of energy metabolism in persister cell survival, we have focused our research on antibiotic-tolerant cells formed during the stationary phase, given that these cells are known to be highly resilient and capable of surviving a variety

of stressors, including antibiotics, and are assumed to be dormant [1,10]. These cells are also referred to as type I persisters, which cannot readily resume growth when diluted in fresh media during the lag phase [1]. Previous studies showed that these persister cells can metabolize specific carbon sources that make them susceptible to aminoglycosides (AG) [29–31]. Their AG susceptibility is due to increased AG uptake, which is facilitated by increased ETC activity and membrane potential [29]. The presence of active energy metabolism in antibiotic-tolerant, non-growing cells may indeed explain their rapid killing by AG in the presence of carbon sources [10,30]. When the knockout strains of global transcriptional regulators (i.e., ArcA, Cra, Crp, DksA, Fnr, Lrp, and RpoS) were screened using the AG potentiation assay in our previous study, the results showed that the panel of carbon sources tested potentiated the AG killing of tolerant cells derived from most knockout strains, except for Δ*crp* and Δ*cyaA* [31]. This can be attributed to the lack of active energy metabolism in these mutant strains, as the Crp/cAMP potentially shapes persister cell metabolism during the stationary phase. Depletion of primary carbon sources activates adenylate cyclase (CyaA) [32], increasing cyclic-AMP (cAMP) levels in cells [33,34]. The cAMP molecules, along with its receptor protein (Crp), activate genes related to the catabolism of secondary carbon sources, potentially supporting cellular functions and energy levels [35–38]. Here, using metabolomics, proteomics, and high-throughput screening of single-gene deletion strains, we have provided evidence that the Crp/cAMP regulatory complex maintains an active state of energy metabolism while downregulating anabolic pathways in the antibiotic-tolerant persister cells.

## RESULTS

**Disruption of the Crp/cAMP complex affects the formation of persister cells at the late stationary phase.** Since Crp/cAMP-mediated metabolic changes can be induced by nutrient depletion during the stationary phase, we wanted to assess the effects of deleting the *crp* and *cyaA* genes (Δ*crp* and Δ*cyaA*) on both persister cell formation and metabolism during this phase. As anticipated, the deletion of the *cyaA* gene resulted in a notable reduction in intracellular cAMP concentration (**Supplementary Fig. 1**). However, the Δ*crp* strain exhibited an increase in cAMP concentration, potentially due to the negative feedback regulatory mechanism of the Crp/cAMP complex for the *cyaA* gene promoter [39,40]. When comparing the growth curves of *E. coli* wild-type (WT), Δ*crp*, and Δ*cyaA* main cultures under identical conditions studied here (see Materials and Methods), all three strains started to enter the stationary phase around 5 hours, with the mutant strains exhibiting slightly lower optical density levels than the WT at this time point (**Supplementary Fig. 2**). Also, our data provide evidence of an increase in cAMP levels in WT cells during their transition into the stationary phase (**Supplementary Fig. 3**), aligning with existing literature [33,34,40]. For type I persister quantification, we diluted cells in the fresh medium (consistent with previous studies [1,10]) at early (t=5h) and late (t=24h) stationary phases and subsequently exposed them to an extended period (20 hours) of ampicillin or ofloxacin treatment (200 µg/mL ampicillin and 5 µg/mL ofloxacin). These treatments were carried out at concentrations surpassing the minimum inhibitory concentrations (MIC), necessary for the selection of antibiotic-tolerant persister cells (**Supplementary Table 1**) [41]. Also, type I persisters, formed during the stationary phase, exhibit a slow transition from a non-growing state to an active state when transferred to a fresh

126 medium in the lag phase [1,10,42,43]; therefore, this transition requires longer antibiotic treatment
127 durations. Moreover, we transferred an equal number of cells from each strain to the fresh
128 medium to ensure consistency in cell numbers. Our findings revealed biphasic kill curves,
129 indicative of persistence phenotypes, with the WT strain showing a notable increase in both
130 ampicillin and ofloxacin-persister cells at the late stationary phase, in contrast to the mutant
131 strains where no such increase was observed (**Fig. 1a,b**). However, no such trend was reported
132 in the early stationary phase (**Fig. 1a,b**). To confirm that the observed decrease in persister
133 levels in the mutant strains in the late stationary phase is solely attributed to the perturbation
134 of the Crp/cAMP regulatory network, we reintroduced *crp* expression to the Δ*crp* strain using a
135 low-copy plasmid carrying the *crp* gene and its promoter. As a control, we utilized an empty
136 vector of the same plasmid. The results demonstrated that the expression of *crp* restored the
137 persister level in the mutant strain, while the plasmid itself had no impact on persister levels
138 (**Supplementary Fig. 4a,b**). Altogether, these findings highlight the significant role of Crp/cAMP
139 in ampicillin and ofloxacin persister formation in the late stationary phase.

140 Ampicillin and ofloxacin, both broad-spectrum antibiotics with a strong dependence on cell
141 metabolism [44], target cell wall synthesis and DNA gyrase activity, respectively. In addition to
142 these two antibiotics, we also quantified aminoglycoside-persister levels in both WT and
143 mutant strains. This was achieved by exposing diluted cells from both early and late stationary
144 phases to 50 µg/mL gentamicin, a concentration exceeding the MIC levels (**Supplementary**
145 **Table 1**). After prolonged gentamicin exposure (20 h), the tolerant cell colonies were found to
146 be below the limit of detection for all strains and conditions (**Fig. 1c,** and **Supplementary Fig.**
147 **4c**). Although bacterial tolerance can vary significantly depending on the specific antibiotics and
148 growth phase used [45], this outcome contrasts starkly with the observed levels of ampicillin and
149 ofloxacin persisters in WT (**Fig. 1**). The mechanism by which aminoglycosides eliminate persister
150 cells in the WT strain may be linked to their metabolism, given that aminoglycoside uptake is an
151 energy-requiring process [29,46], and this aspect will be explored further in the subsequent
152 section.

153 **Crp/cAMP complex governs *E. coli* stationary phase metabolism.** To determine whether the
154 reduced ampicillin and ofloxacin persister levels at the late stationary phase in the mutant
155 strains (**Fig. 1a,b**) are linked to stationary phase metabolism, we utilized untargeted mass
156 spectrometry (MS). This approach facilitated the quantification of metabolites in Δ*crp* cells,
157 allowing for a comparison with WT controls in both the early and late stationary phases. (**Fig.**
158 **2a**). The metabolomics data were subjected to unsupervised hierarchical clustering, and
159 metabolites identified in independent biological replicates of each strain and condition were
160 found to cluster together (**Fig. 2a**), thus confirming the reproducibility of our data.

161 To elucidate the upregulated and downregulated metabolic pathways in the mutant strain as
162 compared to the WT strain, we performed enrichment analyses utilizing MetaboAnalyst [47]. For
163 downregulated pathways, we considered a threshold ratio of 0.5 or lower, where the ratio
164 indicates metabolite levels in the mutant strain relative to the WT (**Supplementary Table 2**).
165 Conversely, for upregulated pathways, the threshold ratio was set at 2 or higher
166 (**Supplementary Table 3**). The enrichment ratio for each pathway was calculated based on the
167 number of metabolite hits compared to the expected hits derived from the chemical structure
168 library [47]. Our extensive comparison of the mutant cells to the WT cells through pathway

enrichment analysis (refer to **Fig. 2b** and **Supplementary Fig. 5, 6 and 7** for pairwise comparison of different conditions) revealed several important findings:

**(i)** During the early stationary phase, we observe a slight downregulation in the abundance of TCA cycle metabolites, including citrate and fumarate, in the Δ*crp* strain compared to WT (**Fig. 2c** and **Supplementary Fig. 5**). However, as the late stationary phase progresses, the downregulation in both TCA cycle and pentose phosphate metabolism becomes more pronounced in the Δ*crp* strain (**Fig. 2b, d**).
**(ii)** The Δ*crp* strain exhibits upregulation of several metabolites compared to WT during both early and late stationary phases, primarily associated with anabolic pathways. Particularly, the upregulation of some of these pathways becomes more pronounced during the late stationary phase. These pathways include crucial metabolites like deoxyribonucleosides and ribonucleosides (which play essential roles in DNA and RNA synthesis), fatty acids and carboxylic acids (the main components of bacterial cell membranes), and peptides (which are linked to protein synthesis) (**Fig. 2b**).
**(iii)** During the early stationary phase, we noticed a significant upregulation in the abundance of intermediate metabolites related to glycolysis, gluconeogenesis, and pyruvate metabolism in mutant cells compared to WT cells (**Fig. 2c**). This observation is not surprising, as the inhibition of the TCA cycle in the mutant strain could potentially redirect metabolic fluxes toward glycolysis and lactate metabolism.

Altogether, our metabolic data indicate that, in the stationary phase, WT cells maintain their energy metabolism to some extent while downregulating their anabolic pathways (**Fig. 2a**). This metabolic state appears to be regulated by the Crp/cAMP complex, as perturbing its function leads to a significant downregulation of energy metabolism and an upregulation in the abundance of anabolic metabolites (**Fig. 2b**).

**Proteomics analysis revealed upregulated pathways in the Δ*crp* strain associated with anabolic metabolism, alongside the downregulation of key proteins in energy metabolism.** Since the Crp/cAMP complex acts as a transcriptional regulator affecting the expression of metabolic proteins whose abundance directly affects cellular metabolites, we performed untargeted proteomics, our second genomic-level study, to further validate our results. Considering the noticeable metabolic alterations observed during the late stationary phase, we utilized MS to quantify proteins in Δ*crp* cells and compared them to WT controls at this stage. The resulting proteomics data were subjected to unsupervised hierarchical clustering, and the proteins identified in independent biological replicates of each strain were found to cluster together, confirming the consistency of our findings (**Supplementary Fig. 8**). By analyzing protein-protein association networks and employing functional enrichment through STRING [48,49], which integrates various functional pathway classification frameworks such as Gene Ontology annotations, KEGG pathways, and UniProt keywords, we pinpointed various upregulated and downregulated pathways in the mutant strain when compared to the WT (**Supplementary Tables 4 and 5**). The upregulated pathways are associated with anabolic metabolism and encompass peptidoglycan metabolic processes, cell wall organization or biogenesis, cellular component organization or biogenesis, regulation of cell shape, cell cycle, and cell division (**Fig. 3a**). Also, the mutant strain displayed downregulated pathways, encompassing glycerol metabolism, TCA cycle, pyruvate metabolism, glycolysis, and various

212 pathways associated with ribosome and transcriptional factor activity (**Fig. 3b)**. Our analysis
213 specifically pinpointed a cluster of proteins involved in energy metabolism and respiratory
214 processes. Notably, this cluster includes GltA, SdhB, SucC, SucD, FrdB, FrdA, AcnA, AceA, and
215 Mdh proteins, which play crucial roles in either the TCA cycle or as membrane-bound
216 components of ETC (**Fig. 3b**). Altogether, the alignment between metabolomics and proteomics
217 analyses provides additional validation for the Crp/cAMP-mediated metabolic state.

218 **Crp/cAMP complex shapes *E. coli* cell proliferation dynamics.** The omics data suggest that the
219 upregulation in the abundance of anabolic metabolites and proteins, particularly those related
220 to cell wall organization or biogenesis, cell cycle, and cell division, in the stationary-phase
221 mutant cells, would likely enhance their ability to resume growth upon transitioning to fresh
222 medium. To investigate this, we utilized a cell proliferation assay that employed an inducible
223 fluorescent protein (mCherry) expression cassette. This assay provided us with the ability to
224 monitor non-growing cells at a single-cell resolution, as described previously [11,50]. The mCherry
225 expression cassette is controlled by an isopropyl ß-D-1-thiogalactopyranoside (IPTG) inducible
226 synthetic T5 promoter that was previously inserted into the chromosome of an *E. coli* strain
227 carrying a *lacI*$^{q}$ promoter mutation [11]. This configuration allowed for precise regulation of
228 mCherry expression using IPTG. Here, we introduced *crp* and *cyaA* deletions into this strain.
229 These deletions reduced the persistence of the mCherry-expressing *E. coli* strain in the late
230 stationary phase (**Supplementary Fig. 9**), consistent with the findings presented in **Fig. 1.** To
231 perform the growth assay, we induced mCherry expression in the main cultures and then
232 washed the cells to remove IPTG. The cells were then inoculated into a fresh medium without
233 IPTG and their growth was analyzed with a flow cytometry. This allowed us to track the dilution
234 of mCherry protein within the cells, which served as an indicator of cell proliferation. As shown
235 in **Fig. 4a**, initially, all cells exhibited high red fluorescence. However, as cells underwent
236 division, the red fluorescence of the overall population decreased in the absence of the inducer
237 (**Fig. 4a**). Notably, within the WT strain, a subpopulation from the late stationary phase cultures
238 displayed constant fluorescence levels, indicating their inability to divide (**Fig. 4b**). In contrast to
239 the WT strain, we did not detect similar subpopulations in the mutant strains (**Fig. 4b**).
240 Additionally, this subpopulation of non-growing cells does not emerge during the early
241 stationary phase cultures (**Fig. 4a**). This observation provides an explanation for the observed
242 reduction in persister levels in these mutant strains in the late stationary phase, as the
243 enrichment of persister cells within these non-growing cell subpopulations was reported in
244 previous studies [30,50,51].

245 To confirm the significance of Crp/cAMP in the formation of non-growing cells, we introduced
246 the expression plasmid carrying the *crp* gene into the Δ*crp* strain. As anticipated, the
247 introduction of the *crp* expression plasmid resulted in the emergence of a non-growing
248 population within the culture, contrasting with the mutant strain containing the empty plasmid
249 vector used as a control (**Supplementary Fig. 10a, b**). The reduced capacity of stationary-phase
250 WT cells to initiate proliferation upon transfer to a fresh medium suggests the possible
251 presence of an extended lag phase in these cells. To investigate this, we employed flow
252 cytometry to precisely quantify cell numbers and generate growth curves for both WT and
253 mutant strains. As anticipated, the growth curve of the WT strain displayed a slower initial
254 growth rate and a prolonged lag phase duration compared to the mutant strains (**Fig. 4c**).

255 Conversely, the mutant strains displayed a shorter lag phase, yet they demonstrated an
256 increased doubling time in the exponential phase compared to WT (**Fig. 4c**), which was also
257 anticipated, considering their decreased reliance on oxidative phosphorylation due to TCA cycle
258 inhibition. Altogether, these results provide additional support and validation for the findings
259 from our metabolomics and proteomics data, as our data reveals a correlation between the
260 abundance of molecules associated with cell division and the ability of the stationary phase
261 cells to resume growth.

262 **Persister cells rely on energy metabolism.** The Crp/cAMP-mediated metabolic state,
263 characterized by increased respiration in WT compared to mutant strains, was further validated
264 using redox sensor green (RSG) dye and a reporter plasmid measuring the promoter activity of
265 succinate:quinone oxidoreductase (SQR) genes. The SQR reporter system [52] employs green
266 fluorescent protein (GFP) expression, regulated by the promoter of the SQR operon, which
267 includes the *sdhA*, *sdhB*, *sdhC*, and *sdhD* subunit genes. The SQR complex plays a vital role in
268 cellular metabolism by catalyzing the oxidation of succinate to fumarate concurrently with the
269 reduction of ubiquinone to ubiquinol, thus directly linking the TCA cycle with the respiratory
270 ETC [40]. Our results indicate an upregulation of the SQR promoter activity in WT cells compared
271 to the mutant strains in the stationary phase, validating the findings from our metabolomics
272 and proteomics data (**Fig. 5a**). The RSG dye, on the other hand, serves as a well-established
273 metabolic indicator, measuring bacterial oxidation-reduction activity, a crucial function
274 involving the ETC driven by the TCA cycle. Once reduced by bacterial reductases, the RSG dye
275 emits a stable green fluorescent signal (**Supplementary Fig. 11**). Our data demonstrate that the
276 redox activities of WT cells are much higher and more heterogeneous compared to those of the
277 mutant strains in the late stationary phase, further corroborating the results from our
278 preceding analyses (**Fig. 5b**). Furthermore, we utilized a methodology that integrates the
279 mCherry expression system, flow cytometry, and ampicillin-mediated cell lysis, to determine
280 whether persister cells in WT still maintain their respiration. In this assay, both the WT and
281 mutant strains carrying the mCherry expression system were exposed to ampicillin after
282 transferring them to a fresh medium. The inducer was added to both growth and treatment
283 cultures to sustain the cells' red signals. Unlike other antibiotics, ampicillin disrupts cell wall
284 synthesis, leading to the lysis of cells upon their resumption of growth. As seen in
285 **Supplementary Fig. 12**, the cells that were lysed lost their mCherry signals. On the other hand,
286 the resilient, tolerant cells that evaded ampicillin-induced lysis maintained their mCherry levels
287 throughout the treatment. In the mutant strains, ampicillin was effective in lysing almost all
288 cells as anticipated, leaving no or small number of intact cells (**Supplementary Fig. 12**).
289 However, in the WT strain, we detected a subpopulation of intact cells throughout the entire
290 treatment period (**Fig. 5c,** and **Supplementary Fig. 12**). While the population-level redox
291 activities of these tolerant intact cells in WT are lower than those of exponential phase cells,
292 they still displayed a significant increase in RSG levels compared to cell populations before
293 antibiotic treatments or untreated control cells subjected to identical conditions **(Fig. 5d),**
294 suggesting that they maintain steady-state energy metabolism. We want to highlight that not
295 all intact cells in the WT strain reported here are persisters. A significant portion comprises
296 'viable but non-culturable' (VBNC) cells, and WT cells exhibit markedly higher VBNC levels than
297 Δ*crp* and Δ*cyaA* mutant strains (**Supplementary Fig. 13**). VBNC cells can be quantified from

intact cells following beta-lactam treatments [30,50]. These cells may exhibit metabolic activities but are unable to readily colonize upon transfer to fresh medium [30,53]. Collectively, our metabolic measurement data (**Fig. 5a, b, c**) aligns with the findings from our omics analyses, and the number of intact cells observed in WT after beta-lactam treatment is consistent with the count of non-growing cells in WT (**Fig. 4b vs Supplementary Fig. 12**). These non-growing cells are anticipated to be less susceptible to lysis by beta-lactams [30,50].

**The genomic-level screening of *E. coli* knockout underscores the significance of energy metabolism in sustaining the viability of persister cells.** Although some metabolic genes, including those encoding the TCA cycle (e.g., *sdhA, sucB, mdh, icd*), have been studied in *E. coli* [9,10,23,54,55], a comprehensive genomic-level screening strategy is necessary to validate which metabolic pathways are truly associated with antibiotic tolerance. To further underscore the importance of energy metabolism, we conducted a high throughput screening of 149 different *E. coli* K-12 BW25113 mutant strains from the Keio knockout library [56]. The selected strains are related to central carbon metabolism, encompassing glycolysis, pentose phosphate pathways, TCA cycle, ETC, ATP synthase, and fermentation pathways (**Fig. 5e**). While the deletion of genes related to glycolysis and pentose phosphate pathways did not affect antibiotic tolerance in the cells, some mutant strains associated with cytochrome bo and quinone oxidoreductase complexes (e.g., *cyo* genes, and *nuoL*) exhibited enhanced tolerance (**Supplementary Table 6**). However, the mutant strains exhibited reduced tolerance to both antibiotics compared to the control K-12 BW25113 WT strain were found to be largely associated with the TCA pathway (*sucA, sucB, lpd, sucC, sucD, sdhA, sdhB, sdhC, sdhD, gltA, acnB, aceE, fumA, mdh* and *fumC*), ETC (*nuoB, nuoC, nuoI, nuoK, nuoM,* and *narV*), ATP synthesis (*atpA, atpB, atpC, atpD, atpE,* and *atpH*), and mixed acid fermentation pathways (*ldhA, fdhF, pta, adhE,* and *frdC*) (**Fig. 5e,** and **Supplementary Table 6**). We acknowledge that the Keio strains were generated in a high-throughput manner, and there might be unknown errors in their genomic DNA. To ensure the reproducibility of our findings, we generated knockout strains for key genes associated with the TCA, ETC, ATP synthase, glycolysis, and pentose phosphate pathway (**Fig. 5f**, see **Supplementary Table 7** for detailed description of genes). We then tested their antibiotic tolerance, and our results were consistent with the omics data and screening outcomes (**Fig. 5f**), confirming the critical role of energy metabolism, specifically the TCA cycle, ETC, and ATP synthase, in bacterial persistence.

## DISCUSSION

Our study highlights the crucial role of the Crp/cAMP complex in maintaining the metabolic state of stationary-phase persister cells, enabling their survival under adverse conditions. Through metabolomics, proteomics, and high-throughput screening of single-gene deletion strains, we substantiated that the Crp/cAMP regulatory complex sustains an active respiratory state while downregulating anabolic pathways in persister cells. This respiratory state is vital for the survival of persister cells, as perturbing the Crp/cAMP complex or respiration significantly reduced persister phenotypes, which may explain the previously reported decrease in antibiotic tolerance in *E. coli* cells cultured under anaerobic conditions [10]. Notably, we observed an upregulation of anabolic metabolites and proteins when the Crp/cAMP regulatory complex was perturbed, particularly those associated with cell wall organization, cell cycle, and cell division, enhancing the ability of stationary-phase mutant cells to resume growth. Although the

341 literature has shown associations between antibiotic tolerance with proteins involved in cell
342 division and the TCA cycle (e.g., SdhA, SucB, Mdh) [9,10,54,55], our study establishes a strong link
343 between these critical cellular processes and the Crp/cAMP complex, providing much-needed
344 clarity in the field. In fact, upon investigating Crp/cAMP regulons via the Ecocyc database [40], we
345 identified that certain metabolic genes, deleted in our *E. coli* K-12 MG1655 background, are
346 potentially regulated by Crp/cAMP (**Supplementary Table 7**), providing additional support for
347 the validity of our omics results. While our discoveries enhance the comprehension of the
348 Crp/cAMP-regulated metabolic network and its implications for antibiotic tolerance, it is
349 essential to address several noteworthy highlights:

350 **(i)** The deletion of *cyaA* resulted in a reduction of cAMP levels, as expected given the role of the
351 CyaA enzyme in cAMP synthesis (**Supplementary Fig. 1**). Conversely, the removal of *crp* led to
352 an increase in cAMP levels compared to those in wild-type cells. Notably, this increase is
353 statistically significant (**Supplementary Fig. 1**), and to the best of our knowledge, this
354 phenomenon has not been described before. We propose two potential reasons for this
355 observation. Firstly, the c*yaA* promoter is recognized to be inhibited by the Crp/cAMP complex
356 [39,40]. The absence of Crp may compromise the formation of the Crp/cAMP complex, potentially
357 enhancing the expression of the CyaA enzyme and consequently increasing cAMP
358 concentration. The second possibility involves a potential inhibition of the cAMP degradation
359 pathway in the Δ*crp* mutant. It is noteworthy that the enzyme responsible for cAMP hydrolysis
360 is cAMP phosphodiesterase, and whether its corresponding gene, *cpdA*, is regulated by the
361 Crp/cAMP complex remains unknown.

362 **(ii)** Our findings reveal substantial heterogeneity in metabolism (measured by RSG) among WT
363 stationary phase cells, contrasting with the more uniform behavior observed in Δ*crp* and Δ*cyaA*
364 strains (**Fig 5b**). We also demonstrated the presence of two distinct populations in WT cells
365 during the late stationary phase: one that resumes rapid growth and another subpopulation
366 that does not resume growth when transferred to a fresh medium (**Fig. 4b**)**.** The absence of this
367 non-growing cell subpopulation in the mutant strains could account for their sensitivity to
368 aminoglycosides. However, the mechanism by which aminoglycosides kill these non-growing
369 cells in the WT strain remains perplexing. The underlying reasons might be linked to their
370 metabolism, as aminoglycoside uptake is an energy-requiring process, relying on the electron
371 flow through membrane-bound respiratory chains [29]. Moreover, persister cells obtained from
372 various antibiotics, such as ampicillin and ofloxacin, in WT *E. coli* were previously found to
373 exhibit sensitivity to aminoglycosides when sugar molecules were introduced into the cultures
374 [29,30]. However, the enhanced sensitivity mediated by sugar molecules was reversed to its
375 original state in a subsequent study when the Crp/cAMP complex was genetically perturbed [31].
376 This can be attributed to the lack of active energy metabolism in these genetically altered
377 strains, as suggested by our comprehensive genomic-level analyses here. While the absence of
378 cell division in non-growing cell subpopulations in WT may suggest a downregulation in
379 anabolic metabolism, their energy metabolism may remain partially active, which could
380 potentially explain the phenomenon of aminoglycoside potentiation. Indeed, our results
381 presented in **Fig. 5d** support this interpretation.

382 **(iii)** Antibiotics are generally effective against proliferating bacteria, leading to the notions that
383 tolerance is linked to temporary growth suppression and that persister cells are dormant

384 phenotypes with repressed metabolism. Our previous studies utilizing a redox sensor and
385 fluorescent-activated cell sorting revealed that, while persister cells were predominantly
386 enriched in cell subpopulations with high redox activities in stationary phase cultures
387 (consistent with our findings) [10], the opposite was observed in exponential phase cultures [11].
388 Indeed, this aligns with the flow diagram presented in **Fig. 5d** in the current study, wherein
389 persister cells exhibit a lower metabolic rate compared to rapidly growing exponential-phase
390 cells and a higher metabolic rate compared to non-growing stationary-phase cells. While
391 several independent studies have demonstrated that persister cells exhibit reduced metabolic
392 activities compared to exponentially growing cells [23,57], the direct comparison of persister cell
393 metabolism to that of exponentially growing cells may not be the best approach. Growing cells
394 have a very high energy output and consume metabolites at a fast pace. Therefore, any
395 comparison between tolerant and non-tolerant cell populations requires proper normalization
396 techniques such as adjusting cellular metabolic activities to the amount of substrate utilized by
397 cells. An example of this normalization was conducted by Heinemann's group [58], demonstrating
398 that ATP production rates per substrate in tolerant cells exceed those of exponentially growing
399 cells.

400 **(iv)** We diluted cells in fresh medium at early and late stationary phases before antibiotic
401 treatments. This step is essential for quantifying type I persisters, as these cells do not readily
402 resume growth upon dilution in the fresh medium during the lag phase [1,10]. We acknowledge
403 that antibiotic tolerance is influenced by various factors, including culture dilutions, media,
404 specific strains, antibiotics tested, treatment durations, and the growth phase during treatment
405 administration. These factors may contribute to variations in reported persister levels observed
406 in the Δ*cyaA* strain during the exponential phase [59–62]. While we did not focus on the
407 exponential growth phase in our study, it is noteworthy that the reduced growth rate during
408 this phase in the mutant strains (**Fig. 4c**) may explain the antibiotic tolerance observed in
409 previous studies involving the *cyaA* deletion [59–62]. The growth disparity noted between mutant
410 and WT strains, particularly evident around 5 hours in our results (**Supplementary Fig. 2**), may
411 also be linked to the ofloxacin persisters observed in the mutant strains at this specific time
412 point (**Fig. 1**). While slow cell growth may indeed correlate with bacterial persistence [63], it is
413 important to note that the persistence associated with perturbations of metabolic genes
414 cannot be solely attributed to the slow growth. In fact, the persistence of these mutant strains
415 should depend on many factors (see **Supplementary Table 7**) as reported by diverse research
416 groups [6,9,10,54,55,64–68]. For instance, in *E. coli*, TCA inactivation was shown to decrease ampicillin
417 and ofloxacin persistence during the lag phase [10], yet it enhances gentamicin tolerance in the
418 exponential phase, which remains unexplained by factors such as cell growth, redox activities,
419 proton motive force (PMF), or ATP levels [69]. Furthermore, gene deletions often trigger
420 pleiotropic effects, leading to unique tolerance mechanisms not evident in wild-type strains. In
421 our Keio screening data analysis, we observed that the deletion of *icd* appeared to enhance
422 persistence (**Supplementary Table 6**), in line with a previous study [23]. The *icd* gene encodes a
423 TCA cycle enzyme, isocitrate dehydrogenase. While it remains unclear whether this observed
424 outcome is attributable to other unseen pleiotropic effects stemming from the *icd* deletion, our
425 data consistently indicates that the most significant reduction in persistence levels occurs with
426 disruptions in energy metabolism. A comprehensive approach, encompassing omics and

427 knockout screening as presented in this study, offers a more complete understanding, revealing
428 the consensus behavior within the entire metabolic network.

429 In conclusion, a significant gap in the current literature is the lack of a comprehensive
430 understanding of how bacterial cell metabolism undergoes changes during the transition to a
431 tolerant state. Identifying the specific metabolic pathways that gain significance for cell survival
432 in this context is crucial. This knowledge can pave the way for the development of more
433 informed and targeted treatment strategies, ultimately enhancing our ability to combat
434 tolerant cells and improve overall treatment outcomes.

435 **MATERIALS AND METHODS**

436 **Bacterial Strains and Plasmids**

437 All experiments were conducted using *E. coli* K-12 MG1655 wild-type (WT) and its derivative
438 strains. *E. coli* K-12 MG1655, MO strains (carrying the mCherry expression system) and pUA66
439 plasmids were obtained from Mark P. Brynildsen at Princeton University. *E. coli* MO strain was
440 used to monitor cell proliferation at single cell level due to its chromosomally integrated
441 isopropyl β-D-1-thiogalactopyranoside (IPTG)-inducible mCherry expression cassette [10,11,30]. *E.*
442 *coli* K-12 BW25113 WT and single deletions were obtained from Dharmacon Keio Collection
443 (Dharmacon, Catalog# OEC4988, Lafayette, CO, USA). The mutant strains in this study were
444 generated using the Datsenko-Wanner method [70]. The pUA66-EV was generated by the removal
445 of *gfp* gene from the plasmid. The *crp* gene with its promoter was cloned into the modified
446 pUA66 plasmid to obtain the pUA66-*crp* expression system. The *SdhABCD* reporter (pMSs201-
447 $P_{sdhABCD}$-*gfp*) was obtained from a previous study [52]. The cloning method was followed
448 according to a standard method from NEB [71]. Genetic modifications were verified by PCR and
449 gene sequencing (Genewiz, South Plainfield, NJ, USA). A complete list of strains, plasmids, and
450 oligonucleotides used in this study is presented in **Supplementary Tables 8** and **9**.

451 **Media, Chemicals, and Culture Conditions**

452 All chemicals used in this study were purchased from Fisher Scientific (Atlanta, GA, USA), VWR
453 International (Pittsburg, PA, USA), or Sigma Aldrich (St. Louis, MO, USA). Luria-Bertani (LB)
454 medium was prepared by combining 5 g of yeast extract, 10 g of tryptone, and 10 g of sodium
455 chloride in 1 L of autoclaved deionized (DI) water. LB agar media was prepared by mixing 40 g of
456 pre-mixed LB agar with 1 L of autoclaved DI water; LB aga media were used to enumerate
457 colony-forming units (CFUs) [10,41,72]. For washing cells and removing chemicals and antibiotics
458 before plating on agar media, 1X Phosphate-Buffered Saline (PBS) was employed. In the
459 persister assay, concentrations of 5 µg/mL of ofloxacin (OFX), 200 µg/mL of ampicillin (AMP),
460 and 50 µg/mL of gentamicin (GEN) were used [29,41,73,74]. The retention of plasmids necessitated
461 50 µg/mL of kanamycin (KAN) in the culture media [10]. Fluorescent protein expression was
462 induced using 1 mM ITPG [10]. Overnight pre-cultures were prepared in 14 mL Falcon test tubes
463 containing 2 mL of LB medium, inoculated from a 25% glycerol cell stock stored at -80°C, and
464 incubated for 24 hours at 37°C with shaking at 250 revolutions per minute (rpm). Main cultures
465 were established by diluting the overnight pre-cultures at a ratio of 1:1000 into 2 mL fresh LB
466 medium in 14 mL Falcon test tubes. Experimental cell cultures were prepared by further dilution

467 of the main cultures into either 25 mL fresh LB medium in 250 mL baffled flasks or 2 mL fresh LB
468 medium in 14 mL Falcon test tubes. Cultures at t=5h and t=24h were defined as early and late
469 stationary phase cultures, respectively. Detailed experimental procedures are outlined below.

470 **Cell growth and persister assays**

471 Main cultures were prepared by diluting the overnight pre-cultures at a ratio of 1:1000 into 2
472 mL of fresh LB medium in 14 mL Falcon test tubes. These cultures were then incubated at 37°C
473 with shaking at 250 rpm. Cell growth was monitored by measuring the optical density at 600 nm
474 wavelength ($OD_{600}$) using a Varioskan LUX Multimode Microplate Reader (Thermo Fisher,
475 Waltham, MA, USA). The plate reader data was collected using Skanlt Software V 5.0. Cell
476 cultures at both early and late stationary phases were collected from the test tubes and
477 transferred to the baffled flasks to achieve ~$5x10^7$ cells/mL. This concentration represents an
478 approximately 100-fold dilution of the WT main culture into a fresh medium within the flask. It
479 is important to highlight that we consistently employed flow cytometry to quantify the initial
480 cell count (refer to the section "Monitoring cell division" for comprehensive details). As needed,
481 adjustments in cell number-to-volume were executed to ensure the same cell number among
482 both WT and mutant strains. These cultures were then treated with antibiotics at the indicated
483 concentrations and were cultured with shaking at 37°C for 20 hours. After the treatment, a 1 mL
484 sample from each flask was transferred to a microcentrifuge tube and centrifuged at 13,300
485 rpm (17,000 x gravitational force or g). The supernatant (900 µL) was removed, and the cells
486 were washed twice with 1X PBS to eliminate antibiotics from the sample. Following the washes,
487 100 µL of 1X PBS was used to resuspend the cells. A 10 µL sample of this cell suspension was
488 serially diluted in a 96-well round-bottom plate. Then, 10 µL from each dilution was spotted on
489 an agar plate, and the remaining 90 µL from the most concentrated well was plated to ensure
490 viable cell detection down to a limit equivalent to 1 CFU/mL. These plates were incubated for 16
491 hours at 37°C to allow CFUs to develop.

492 **cAMP profile assay**

493 An overnight pre-culture of *E. coli* K-12 MG1655 WT was prepared in test tubes with 2 mL of LB
494 medium. The culture was incubated at 37°C with shaking at 250 rpm for 24 hours. For the
495 experimental cultures, a 1:1000 dilution was made in fresh medium. At time-points 0, 2, 4, 6, 8
496 and 24h, 100 µL of the experimental culture was washed with cold 1X PBS. After centrifuging at
497 13,300 rpm (17,000 x gravitational force or g), the supernatant was removed. The cells were
498 then resuspended in 100 µL of cell lysis buffer from the Cyclic AMP XP® Assay Kit (Catalog#
499 4339S, Cell Signaling Technology, Danvers, MA, USA) on ice for 10 minutes. Next, 50 µL of lysed
500 cells was mixed with the kit's horseradish peroxidase (HRP)-linked cAMP solution in the cAMP
501 assay plate. This mixture was incubated at room temperature for 3 hours on a plate shaker at
502 250 rpm. Following the 3-hour incubation, the plate content was discarded, and the plate was
503 washed four times with the kit's Wash Buffer. Then, 100 µL of tetramethylbenzidine (TMB)
504 substrate was added to allow color development, and after 30 minutes, 100 µL of the stop
505 solution provided by the kit was added. The absorbance was measured at 450 nm using a plate
506 reader. The standard curve was prepared using the same conditions and the standard cAMP
507 solutions provided by the kit to determine cAMP concentrations.

508 **Metabolomics**

509 Metabolites from both Δ*crp* and WT cells were analyzed at the Metabolon, Inc., facility
510 (Morrisville, NC, USA). Cells were cultured until the early stationary phase and late stationary
511 phase at 37°C with shaking at 250 rpm. Afterward, cells were collected through centrifugation at
512 4700 rpm at 37°C for 15 minutes, yielding a pellet of approximately 100 µL containing around
513 $10^{10}$ cells. Subsequently, the cells were washed once with 1X PBS and then centrifuged (13,000
514 rpm, 3 minutes at 4°C). Following this, they were frozen in an ethanol/dry ice bath for 10
515 minutes. The extracts from both mutant and WT cells were subjected to analysis using ultra-
516 high-performance liquid chromatography-tandem accurate mass spectrometry (MS), a process
517 aimed at identifying a wide range of metabolites. Sample extraction, preparation, instrument
518 settings, and conditions for the MS platform adhered to Metabolon's protocols (as detailed in
519 our previous study) [75]. To identify the sample's metabolites among potential false positives from
520 instrument noise, process artifacts, and redundant ion features, the results were cross-
521 referenced with Metabolon's extensive metabolite library (standards). Data normalization was
522 carried out based on protein concentration, determined using the Bradford assay. The
523 significant difference between mutant and WT was identified using Welch's two-sample t-test.
524 Further analysis involved pathway enrichment assessment using MetaboAnalyst [47]. This involved
525 inputting the upregulated and downregulated metabolites based on chosen thresholds. A
526 comprehensive overview of metabolite measurements, pathway enrichment, statistical
527 analyses, and data representations can be found in our previously published study [75].

528 **Proteomics**

529 Overnight cultures for both WT and Δ*crp* were prepared using 2 mL of LB medium. Incubation
530 was carried out at 37°C and 250 rpm for 24 hours. The following day, the main cultures were
531 established under the same conditions, using a 1000-fold dilution of the overnight culture in 2
532 mL fresh LB medium. After 24 hours, the $OD_{600}$ of both WT and mutant strains was measured
533 and adjusted to an $OD_{600}$ of 2.5. For further processing, 2 mL of the main culture was washed
534 twice with cold 1X PBS, maintaining the cold environment throughout. Centrifugation conditions
535 were set at 4°C, 13,000 rpm for 3 minutes. Before the final centrifugation, a cell count was
536 conducted using flow cytometry. This involved using 10 µL of washed culture and 990 µL of 1X
537 PBS. Subsequent to centrifugation, the pellets were collected. Cell lysis was carried out using
538 300 µL of NEBExpress® *E. coli* Lysis Reagent (Catalog# P8116S, Ipswich, MA, USA) at room
539 temperature for 30 minutes. Following this, the lysed samples were centrifuged at 16,600 x g for
540 10 minutes, and 250 µL of supernatants were collected from each sample for the assay. The
541 total protein concentration of the supernatants was determined using the bicinchoninic acid
542 (BCA) assay (Catalog# 23225, Thermo Fisher Scientific, Waltham, MA, USA). In a 96-well plate,
543 25 µL of each cell lysate sample, diluted 5 and 10 times with ultra-pure DI water, were loaded
544 into each well. Subsequently, 200 µL of the BCA working reagent (50:1, Reagent A:B) was added
545 to each well and mixed on a plate shaker for 30 seconds. The plate was then incubated at 37°C
546 for 30 minutes, followed by cooling for 5 minutes at room temperature, shielded from light. The
547 absorbance was finally measured at 562 nm using a plate reader, and the total protein
548 concentration in each sample was calculated using a standard curve prepared from standard

549 protein solutions. Protein analysis for both WT and mutant was conducted by the proteomics
550 service at UT Health's Clinical and Translational Proteomics Service Center (Houston, TX). The
551 samples underwent acetone precipitation, during which proteins were precipitated by exposing
552 them to -20°C for 3 hours. Following this, a centrifugation step at 12,000 g for 5 minutes
553 separated the precipitated pellets. These pellets were subsequently subjected to denaturation
554 and reduction using a mixture containing 30 µL of 6 M urea, 20 mM DTT in 150 mM Tris HCl (pH
555 8.0) at 37°C for 40 minutes. Afterward, alkylation was carried out with 40 mM iodoacetamide in
556 the absence of light for 30 minutes. To prepare for digestion, the reaction mixture was diluted
557 10-fold using 50 mM Tris-HCl (pH 8.0) and then incubated overnight at 37°C with trypsin at a
558 1:30 enzyme-to-substrate ratio. The digestion process was terminated by adding an equal
559 volume of 2% formic acid, followed by desalting using Waters Oasis HLB 1 mL reverse phase
560 cartridges, following the vendor's recommended procedure. Finally, the eluates were dried
561 using vacuum centrifugation. Approximately 1 µg of the tryptic digest, prepared in a solution
562 containing 2% acetonitrile and 0.1% formic acid in water, underwent analysis using LC/MS/MS.
563 The instrument used was the Orbitrap Fusion™ Tribrid™ mass spectrometer by Thermo
564 Scientific™, connected to a Dionex UltiMate 3000 Binary RSLCnano System. The separation of
565 peptides occurred on an analytical C18 column with dimensions of 100 µm ID x 25 cm, featuring
566 5 µm particles and an 18 Å pore size. Peptides were eluted at a flow rate of 350 nL/min. The
567 gradient conditions applied were as follows: a gradient starting from 3% B and increasing to 22%
568 B over a duration of 90 minutes, followed by a step to 22%-35% B for 10 minutes, then another
569 step to 35%-90% B for 10 minutes, and finally, maintaining 90% B for an additional 10 minutes
570 (Solvent A was composed of 0.1% formic acid in water, while solvent B contained 0.1% formic
571 acid in acetonitrile). The peptides were analyzed using a data-dependent acquisition method.
572 The Orbitrap Fusion MS operated by measuring FTMS1 spectra with a resolution of 120,000
573 FWHM, scanning in the m/z range of 350-1500, using an AGC target set to 2E5, and with a
574 maximum injection time of 50 ms. Within a maximum cycle time of 3 sec, ITMS2 spectra were
575 collected in rapid scan mode. High Collision Dissociation (HCD) was employed with a normalized
576 collision energy (NCE) of 34, an isolation window of 1.6 m/z, an AGC target set to 1E4, and a
577 maximum injection time of 35 ms. Dynamic exclusion was implemented for a duration of 35 sec
578 to prevent repeated analysis of the same ions. For the experimental analysis, the Thermo
579 Scientific™ Proteome Discoverer™ software version 1.4 was utilized to process the raw data
580 files. The spectra were subjected to analysis against the *E. coli* proteome database (Swiss-Prot
581 29,161) through the Sequest HT search engine. Additionally, the spectra were compared against
582 a decoy database, employing a target false discovery rate (FDR) of 1% for stringent criteria and
583 5% for more relaxed criteria. The enzymatic cleavage allowance for trypsin included up to two
584 potential missed cleavages. The MS tolerance was defined as 10 ppm, while the MS/MS
585 tolerance was set at 0.6 Da. Fixed modification involved carbamidomethylation on cysteine
586 residues, and variable modifications encompassed methionine oxidation and asparagine
587 deamidation. For proteomics data processing and fold change calculations, the approaches
588 were essentially followed by the method paper from Aguilan *et al* [76] . Then, the STRING tool V
589 12.0 [48,49] was employed to find the significant networks among input proteins. To generate the

590 protein network and pathway enrichment analysis, we input the protein identifiers (Accession
591 numbers) for upregulated or downregulated proteins with at least a 2-fold increase or
592 reduction, respectively. *E. coli* K-12 was selected as the organism of interest. We opted for
593 evidence as the criterion for network edges, prioritizing the type of interaction evidence,
594 helping us conduct an automated pathway-enrichment analysis, centering on the entered
595 proteins and identifying pathways that occurred more frequently than expected. This analysis
596 was grounded in the statistical background of the entire genome and encompasses various
597 functional pathway classification frameworks, such as Gene Ontology annotations, KEGG
598 pathways, and Uniprot keywords, as detailed elsewhere [48,49]. In pathway enrichment analysis,
599 the "strength score," calculated as Log10(observed/expected), serves to assess the degree or
600 significance of enrichment within a specific biological pathway. This metric reflects the
601 magnitude of the enrichment effect, with a higher score indicating stronger enrichment. The
602 score is derived from the ratio of i) annotated proteins in the network for a given term to ii) the
603 expected number of proteins annotated with the same term in a random network of equivalent
604 size [48,49]. To gauge the significance of enrichment, False Discovery Rate (FDR) is employed. FDR
605 scores represent p-values corrected for multiple testing within each category using the
606 Benjamini–Hochberg procedure [48,49].
607 **Monitoring cell division**
608 To monitor cell division and quantify non-growing cells, we utilized inducible fluorescent protein
609 (mCherry) expression. Overnight pre-cultures of *E. coli* MO were prepared with 2 mL of LB
610 medium containing 1 mM of ITPG. These cultures were grown in test tubes at 37°C with shaking
611 at 250 rpm for 24 hours. Main cultures were established by diluting the overnight pre-cultures
612 (at a ratio of 1:1000) into 2 mL of fresh LB medium in 14 mL Falcon test tubes. These cultures
613 were incubated at 37°C with shaking at 250 rpm. Cells were allowed to grow until they reached
614 the early stationary phase and the late stationary phase. The mCherry positive cells were then
615 collected, washed twice with 1X PBS to remove the ITPG from the culture, and subsequently re-
616 suspended in fresh 2 ml LB media in test tubes to achieve ~$5x10^7$ cells/mL. This concentration
617 represents an approximately 100-fold dilution. When needed, adjustments in cell number-to-
618 volume were made to ensure the same cell number among both WT and mutant strains. In the
619 experimental culture test tubes, 2 mL of LB medium were added, and the volume of washed
620 cells was inoculated to achieve an $OD_{600}$ of 0.0286. The culture was then incubated at 37°C with
621 shaking at 250 rpm. At specific time points (0, 1, 2, and 2.5h), cells were collected and re-
622 suspended in 1X PBS to measure their fluorescent protein content using flow cytometry. For
623 flow cytometry analysis, cells were collected and diluted to a desired cell density (~$10^6$-$10^7$
624 cells/mL) in 1 mL of 1X PBS in flow cytometry tubes (5 mL round-bottom Falcon tubes, size: 12 x
625 75 mm). The flow cytometry analysis was conducted using a NovoCyte 3000RYB instrument
626 (ACEA Bioscience Inc., San Diego, CA, USA). During flow cytometry analysis, a slow sample flow
627 rate of 14 µL/min was chosen, along with a sample stream diameter (core diameter) of 7.7 µm.
628 The instrument maintained a constant sheath flow rate of 6.5 mL/min. The core diameter was
629 calculated using the ratio of the sample flow rate to the sheath flow rate. These specific
630 conditions were selected to achieve improved data resolution for the size of *E. coli* cells. Flow

631 diagrams utilized forward and side scatter signals from viable cells, alongside a control of
632 solvent devoid of cells, to ascertain the presence of cells. For the flow cytometry analysis, cells
633 were excited at a 561 nm wavelength, and the red fluorescence was detected using a 615/20
634 nm bandpass filter.

635 **Cell growth measured by flow cytometry**

636 Overnight cultures of *E. coli* K-12 MG1655 MO WT and MO mutant strains were diluted at a
637 ratio of 1:1000 into 2 mL of fresh LB medium, placed in 14 mL Falcon test tubes, and incubated
638 at 37°C with shaking at 250 rpm for 24 hours. For the main cultures, a similar strategy was
639 employed. The cultures were diluted at a ratio of 1:100 into 2 mL of fresh LB medium in 14 mL
640 Falcon test tubes. These cultures were then incubated at 37°C with shaking at 250 rpm. At
641 specific time points, including t=0, 20 min, 40 min, and 1 to 5h, the cell growth was halted. This
642 was achieved by diluting the cells in 1X PBS containing 25 µg/mL of chloramphenicol (CAM). The
643 CAM treatment allowed for subsequent analysis without further division. Flow cytometry was
644 then utilized to measure the number of cells at each of these time points. This approach
645 provided insight into cell division dynamics and allowed for the quantification of cell
646 populations under specific conditions.

647 **Fluorescent protein expression assay for reporter genes**

648 Mutant and control strains were derived from *E. coli* K-12 MG1655 and carried pMSs201-*gfp*
649 plasmids incorporating a $P_{sdhABCD}$ gene promoter. Overnight pre-cultures were prepared using 2
650 mL of LB medium supplemented with 50 µg/mL KAN. These cultures were incubated in test
651 tubes within a shaker at 37°C for 24 hours. Main cultures were established by diluting the
652 overnight pre-cultures at a ratio of 1:1000 into 2 mL of fresh LB medium within 14 mL Falcon
653 test tubes. These main cultures were maintained at 37°C with shaking at 250 rpm. Cell cultures
654 at the desired growth phase were collected and then diluted to attain a desired cell density of
655 around $10^6$-$10^7$ cells/mL in 1mL of 1X PBS within flow cytometry tubes. This allowed for
656 subsequent flow cytometry analysis, using the same conditions as described earlier for
657 monitoring cell division (refer to "Monitoring cell division"). During analysis, a laser emitting
658 light at 488 nm was used to excite the cells, and the resulting green fluorescence was detected
659 using a 530/30 nm bandpass filter. This setup enabled the examination of the fluorescence
660 patterns of the cells, offering insights into their dynamics under different conditions.

661 **Redox Sensor Green assay**

662 To gauge bacterial metabolic activity, we employed the Redox Sensor Green (RSG) dye from
663 Thermo Fisher (Catalog# B34954, Thermo Fisher Scientific, Waltham, MA). *E. coli* K-12 MG1655
664 WT and mutant cells from the desired growth phase were diluted at a ratio of 1:100 in 1 mL of
665 1X PBS. To this solution, 1 µL of the RSG dye was added to flow cytometry tubes. After a brief
666 vortexing to ensure uniform mixing, the samples were incubated at 37°C in darkness for 10
667 minutes. Subsequently, these samples were subjected to flow cytometry analysis. For the flow
668 cytometry analysis, the same methodology as employed in "Monitoring cell division" was
669 followed, with one variation. Cells were excited at 488 nm during analysis, and the resulting
670 green fluorescence was detected using a 530/30 nm bandpass filter. This setup allowed us to
671 assess the fluorescence patterns, reflecting the metabolic activity of the bacterial cells under

672 different conditions. As a control measure, cells were treated with 20 µM of carbonyl cyanide
673 m-chlorophenyl hydrazone (CCCP) for 5 minutes before the addition of the RSG dye. This served
674 to validate the assay's sensitivity to changes in metabolic activity (**Supplementary Fig. 11**).

675 **Metabolic activity of non-lysing cells and VBNC cell quantification**

676 Overnight cultures of *E. coli* K-12 MG1655 MO WT and MO mutant strains were diluted at a
677 ratio of 1:1000 into 2 mL of fresh LB medium supplemented with 1 mM ITPG. These cultures
678 were established in 14 mL Falcon test tubes and incubated at 37°C with shaking at 250 rpm for
679 24 hours. Treatment cultures were prepared by diluting the main cultures at a ratio of 1:100 into
680 25 mL of fresh LB medium supplemented with 1 mM ITPG. These cultures were set up in 250 mL
681 baffled flasks and contained 200 µg/mL AMP. They were then cultured at 37°C with shaking at
682 250 rpm for 20 hours. Both before and after the treatment, 1 mL samples were collected from
683 the cultures. These samples were subjected to a washing procedure with 1X PBS to eliminate
684 the antibiotic present in the samples. The washed cells were then resuspended in 1 mL of 1X
685 PBS within flow cytometry tubes. To measure the metabolic activity of the non-lysing cells, the
686 RSG dye was employed as described above. Intact cells (following antibiotic treatment), stained
687 as live with RSG, comprised both persister and VBNC cells. Persister levels were quantified by
688 plating the cells on an agar medium, as described previously [30]. As VBNC cells cannot grow on
689 agar medium, their enumeration involved subtracting the number of persister cells from the
690 total number of intact cells.

691 **Screening *E. coli* (K-12 BW25113) Keio Knockout Collection**

692 Overnight cultures of individual mutant strains, along with their parental strain K-12 BW25113
693 WT harboring a kanamycin-resistant marker, were diluted at a ratio of 1:1000 in fresh LB
694 medium containing 50 µg/mL of KAN. This was done in 14 mL Falcon test tubes and the cultures
695 were then incubated at 37°C with shaking at 250 rpm. Upon reaching the late stationary phase,
696 cells were further diluted at a ratio of 1:100 in fresh medium supplemented with antibiotics at
697 specified concentrations. These cultures were once again incubated at 37°C with shaking for 20
698 hours. Following the 20-hour treatment period, the same methodology described in the section
699 "Cell growth and persister assays" was employed to quantify the number of persisters. This
700 approach allowed for an assessment of the impact of antibiotics on the formation of persister
701 cells for both mutant strains and the parental K-12 BW25113 WT strain.

702 **Persister quantitation in *E. coli* K-12 MG1655 single gene deletions**

703 Overnight cultures of mutant strains were diluted at a ratio of 1:1000 in 14 mL Falcon test tubes
704 containing 2 mL of LB medium. These cultures were then incubated at 37°C with shaking at 250
705 rpm. Upon reaching the late stationary phase, cells were diluted at a ratio of 1:100 in fresh
706 medium supplemented with antibiotics at specified concentrations. The cultures were once
707 again subjected to shaking at 37°C for 20 hours. The same method described earlier, referred to
708 as "Cell growth and persister assays," was employed to quantify the number of persister cells
709 resulting from this treatment. This approach allowed for the assessment of the impact of
710 antibiotic exposure on persister cell formation within the mutant strains.

711 **Statistics and reproducibility**

712 A nonlinear logarithmic model was employed to create biphasic kill curves [18,77]. The significance

of these kill curves was determined through the utilization of F statistics [18,77]. Metabolomics data were subjected to analysis using Welch's two-sample t-test in order to identify metabolites that significantly differed between the control and mutant groups [78]. For all experiments, a minimum of three independent biological replicates were conducted, unless explicitly stated otherwise. In each figure (excluding flow diagrams), the data for each time point are represented as the mean value accompanied by the standard deviation. In terms of statistical significance analysis, the designated threshold values for P were set as follows: *P < 0.05, **P < 0.01, ***P < 0.001, and ****P < 0.0001. All figures were generated using GraphPad Prism 10.3.0. The statistical analyses were carried out using the statistical functions of GraphPad Prism 10.3.0. For the clustering of metabolomics and proteomics data, the "Clustergram" function of MATLAB (V R2020b) was employed. FlowJo (V 10.8.1) was the tool used to analyze the data acquired from flow cytometry.

**Acknowledgment**

The authors would like to thank the members of Orman Lab for their help. This study was supported by NSF CAREER 2044375 and NIH/NIAID R01-AI143643.

**Contributions**

H.N. and M.A.O. conceived and designed the study. H.N. and S.G.M. performed the experiments. H.N., S.G.M., A.A., and M.A.O. analyzed the data and wrote the paper. All authors have read and approved the manuscript. Metabolomics experiments and data analysis were conducted by Metabolon, Inc., under a service fee. Proteomics experiments were carried out by UT Health's Clinical and Translational Proteomics Service Center, under a service fee. The proteomics data analysis was performed by coauthor A.A.

**Corresponding author**

Correspondence to Mehmet A. Orman (morman@central.uh.edu)

**Declaration of interests**

The authors declare no competing interests.

**Supplementary file**

The supplementary file contains Supplementary Figures and Tables.

**Data availability**

All data in this manuscript can be found in either Main text or Supplementary file.

**References**

1. Balaban, N. Q., Merrin, J., Chait, R., Kowalik, L. & Leibler, S. Bacterial persistence as a phenotypic switch. *Science (1979)* **305**, 1622–1625 (2004).
2. Lewis, K. Persister cells. *Annual Review of Microbiology* vol. 64 Preprint at https://doi.org/10.1146/annurev.micro.112408.134306 (2010).
3. Adams, K. N. *et al.* Drug tolerance in replicating mycobacteria mediated by a macrophage-induced efflux mechanism. *Cell* **145**, 39–53 (2011).
4. Wakamoto, Y. *et al.* Dynamic Persistence of Antibiotic-Stressed Mycobacteria. *Science (1979)* **339**, 91–95 (2013).

754 5. Arnoldini, M. *et al.* Bistable Expression of Virulence Genes in Salmonella Leads to the
755 Formation of an Antibiotic-Tolerant Subpopulation. *PLoS Biol* **12**, e1001928 (2014).
756 6. Shan, Y., Lazinski, D., Rowe, S., Camilli, A. & Lewis, K. Genetic Basis of Persister Tolerance
757 to Aminoglycosides in Escherichia coli. *mBio* **6**, (2015).
758 7. Mok, W. W. K., Park, J. O., Rabinowitz, J. D. & Brynildsen, M. P. RNA Futile Cycling in
759 Model Persisters Derived from MazF Accumulation. *mBio* **6**, (2015).
760 8. Hossain, T., Singh, A. & Butzin, N. C. *Escherichia coli* cells are primed for survival before
761 lethal antibiotic stress. *Microbiol Spectr* **11**, (2023).
762 9. Ma, C. *et al.* Energy production genes sucB and ubiF are involved in persister survival and
763 tolerance to multiple antibiotics and stresses in Escherichia coli. *FEMS Microbiol Lett* **303**,
764 33–40 (2010).
765 10. Orman, M. A. & Brynildsen, M. P. Inhibition of stationary phase respiration impairs
766 persister formation in E. coli. *Nat Commun* **6**, 7983 (2015).
767 11. Orman, M. A. & Brynildsen, M. P. Dormancy is not necessary or sufficient for bacterial
768 persistence. *Antimicrob Agents Chemother* **57**, 3230–3239 (2013).
769 12. Michiels, J. E., Van den Bergh, B., Verstraeten, N. & Michiels, J. Molecular mechanisms
770 and clinical implications of bacterial persistence. *Drug Resistance Updates* **29**, 76–89
771 (2016).
772 13. Huemer, M., Mairpady Shambat, S., Brugger, S. D. & Zinkernagel, A. S. Antibiotic
773 resistance and persistence—Implications for human health and treatment perspectives.
774 *EMBO Rep* **21**, (2020).
775 14. Murray, C. J. L. *et al.* Global burden of bacterial antimicrobial resistance in 2019: a
776 systematic analysis. *The Lancet* **399**, 629–655 (2022).
777 15. Fisher, R. A., Gollan, B. & Helaine, S. Persistent bacterial infections and persister cells.
778 *Nat Rev Microbiol* **15**, 453–464 (2017).
779 16. Barrett, T. C., Mok, W. W. K., Murawski, A. M. & Brynildsen, M. P. Enhanced antibiotic
780 resistance development from fluoroquinolone persisters after a single exposure to
781 antibiotic. *Nat Commun* **10**, 1177 (2019).
782 17. Levin-Reisman, I. *et al.* Antibiotic tolerance facilitates the evolution of resistance. *Science*
783 *(1979)* **355**, 826–830 (2017).
784 18. Windels, E. M. *et al.* Bacterial persistence promotes the evolution of antibiotic resistance
785 by increasing survival and mutation rates. *ISME J* **13**, 1239–1251 (2019).
786 19. Warburg, O. The metabolism of carcinoma cells. *J Cancer Res* **9**, 148–163 (1925).
787 20. Hanahan, D. & Weinberg, R. A. Hallmarks of cancer: the next generation. *Cell* **144**, 646–
788 674 (2011).
789 21. Vasan, K., Werner, M. & Chandel, N. S. Mitochondrial metabolism as a target for cancer
790 therapy. *Cell Metab* **32**, 341–352 (2020).
791 22. Porporato, P. E., Filigheddu, N., Pedro, J. M. B.-S., Kroemer, G. & Galluzzi, L.
792 Mitochondrial metabolism and cancer. *Cell Res* **28**, 265–280 (2018).
793 23. Manuse, S. *et al.* Bacterial persisters are a stochastically formed subpopulation of low-
794 energy cells. *PLoS Biol* **19**, e3001194 (2021).
795 24. Mohiuddin, S. G., Kavousi, P. & Orman, M. A. Flow-cytometry analysis reveals persister
796 resuscitation characteristics. *BMC Microbiol* **20**, 202 (2020).

797 25. Goormaghtigh, F. & Van Melderen, L. Single-cell imaging and characterization of
798 Escherichia coli persister cells to ofloxacin in exponential cultures. *Sci Adv* **5**, eaav9462
799 (2019).
800 26. Conlon, B. P. *et al.* Persister formation in Staphylococcus aureus is associated with ATP
801 depletion. *Nat Microbiol* **1**, 1–7 (2016).
802 27. Prax, M. & Bertram, R. Metabolic aspects of bacterial persisters. *Front Cell Infect*
803 *Microbiol* **4**, 148 (2014).
804 28. Amato, S. M. *et al.* The role of metabolism in bacterial persistence. *Front Microbiol* **5**, 70
805 (2014).
806 29. Allison, K. R., Brynildsen, M. P. & Collins, J. J. Metabolite-enabled eradication of bacterial
807 persisters by aminoglycosides. *Nature* **473**, 216–220 (2011).
808 30. Orman, M. A. & Brynildsen, M. P. Establishment of a method to rapidly assay bacterial
809 persister metabolism. *Antimicrob Agents Chemother* **57**, 4398–4409 (2013).
810 31. Mok, W. W. K., Orman, M. A. & Brynildsen, M. P. Impacts of global transcriptional
811 regulators on persister metabolism. *Antimicrob Agents Chemother* **59**, 2713–2719 (2015).
812 32. Pastan, I. & Perlman, R. Cyclic Adenosine Monophosphate in Bacteria: In many bacteria
813 the synthesis of inducible enzymes requires this cyclic nucleotide. *Science (1979)* **169**,
814 339–344 (1970).
815 33. Bettenbrock, K. *et al.* Correlation between growth rates, EIIACrr phosphorylation, and
816 intracellular cyclic AMP levels in Escherichia coli K-12. *J Bacteriol* **189**, 6891–6900 (2007).
817 34. Park, Y.-H., Lee, B. R., Seok, Y.-J. & Peterkofsky, A. In vitro reconstitution of catabolite
818 repression in Escherichia coli. *Journal of Biological Chemistry* **281**, 6448–6454 (2006).
819 35. Deutscher, J. The mechanisms of carbon catabolite repression in bacteria. *Curr Opin*
820 *Microbiol* **11**, 87–93 (2008).
821 36. Fic, E. *et al.* cAMP receptor protein from Escherichia coli as a model of signal
822 transduction in proteins–a review. *Microb Physiol* **17**, 1–11 (2009).
823 37. Görke, B. & Stülke, J. Carbon catabolite repression in bacteria: many ways to make the
824 most out of nutrients. *Nat Rev Microbiol* **6**, 613–624 (2008).
825 38. Kolb, A., Busby, S., Buc, H., Garges, S. & Adhya, S. Transcriptional regulation by cAMP and
826 its receptor protein. *Annu Rev Biochem* **62**, 749–797 (1993).
827 39. Majerfeld, I. H., Miller, D., Spitz, E. & Rickenberg, H. V. Regulation of the synthesis of
828 adenylate cyclase in Escherichia coli by the cAMP — cAMP receptor protein complex.
829 *Mol Gen Genet* **181**, 470–475 (1981).
830 40. Keseler, I. M. EcoCyc: a comprehensive database resource for Escherichia coli. *Nucleic*
831 *Acids Res* **33**, D334–D337 (2004).
832 41. Keren, I., Kaldalu, N., Spoering, A., Wang, Y. & Lewis, K. Persister cells and tolerance to
833 antimicrobials. *FEMS Microbiol Lett* **230**, 13–18 (2004).
834 42. Vulin, C., Leimer, N., Huemer, M., Ackermann, M. & Zinkernagel, A. S. Prolonged bacterial
835 lag time results in small colony variants that represent a sub-population of persisters.
836 *Nat Commun* **9**, 4074 (2018).
837 43. Jõers, A. & Tenson, T. Growth resumption from stationary phase reveals memory in
838 Escherichia coli cultures. *Sci Rep* **6**, 24055 (2016).

839 44. Zheng, E. J., Stokes, J. M. & Collins, J. J. Eradicating Bacterial Persisters with Combinations
840 of Strongly and Weakly Metabolism-Dependent Antibiotics. *Cell Chem Biol* (2020)
841 doi:10.1016/j.chembiol.2020.08.015.
842 45. Hofsteenge, N., van Nimwegen, E. & Silander, O. K. Quantitative analysis of persister
843 fractions suggests different mechanisms of formation among environmental isolates of E.
844 coli. *BMC Microbiol* **13**, 25 (2013).
845 46. Taber, H. W., Mueller, J. P., Miller, P. F. & Arrow, A. S. Bacterial uptake of aminoglycoside
846 antibiotics. *Microbiol Rev* **51**, 439–457 (1987).
847 47. Lu, Y., Pang, Z. & Xia, J. Comprehensive investigation of pathway enrichment methods for
848 functional interpretation of LC–MS global metabolomics data. *Brief Bioinform* **24**,
849 bbac553 (2023).
850 48. Szklarczyk, D. *et al.* The STRING database in 2023: protein–protein association networks
851 and functional enrichment analyses for any sequenced genome of interest. *Nucleic Acids*
852 *Res* **51**, D638–D646 (2023).
853 49. Szklarczyk, D. *et al.* The STRING database in 2021: customizable protein–protein
854 networks, and functional characterization of user-uploaded gene/measurement sets.
855 *Nucleic Acids Res* **49**, D605–D612 (2021).
856 50. Roostalu, J., J\~oers, A., Luidalepp, H., Kaldalu, N. & Tenson, T. Cell division in Escherichia
857 coli cultures monitored at single cell resolution. *BMC Microbiol* **8**, 1–14 (2008).
858 51. Joers, A., Kaldalu, N. & Tenson, T. The frequency of persisters in Escherichia coli reflects
859 the kinetics of awakening from dormancy. *J Bacteriol* **192**, 3379–3384 (2010).
860 52. Zaslaver, A. *et al.* A comprehensive library of fluorescent transcriptional reporters for
861 Escherichia coli. *Nat Methods* **3**, 623–628 (2006).
862 53. Ayrapetyan, M., Williams, T. & Oliver, J. D. Relationship between the Viable but
863 Nonculturable State and Antibiotic Persister Cells. *J Bacteriol* **200**, (2018).
864 54. Luidalepp, H., Joers, A., Kaldalu, N. & Tenson, T. Age of inoculum strongly influences
865 persister frequency and can mask effects of mutations implicated in altered persistence.
866 *J Bacteriol* **193**, 3598–3605 (2011).
867 55. Yu, J., Liu, Y., Yin, H. & Chang, Z. Regrowth-delay body as a bacterial subcellular structure
868 marking multidrug-tolerant persisters. *Cell Discov* **5**, 8 (2019).
869 56. Baba, T. *et al.* Construction of *Escherichia coli* K-12 in-frame, single-gene knockout
870 mutants: the Keio collection. *Mol Syst Biol* **2**, (2006).
871 57. Shan, Y. *et al.* ATP-dependent persister formation in Escherichia coli. *mBio* **8**, 10–1128
872 (2017).
873 58. Radzikowski, J. L. *et al.* Bacterial persistence is an active σS stress response to metabolic
874 flux limitation. *Mol Syst Biol* **12**, 882 (2016).
875 59. Chu, W. *et al.* Indole production promotes Escherichia coli mixed-culture growth with
876 Pseudomonas aeruginosa by inhibiting quorum signaling. *Appl Environ Microbiol* **78**, 411–
877 419 (2012).
878 60. Molina-Quiroz, R. C. *et al.* Cyclic AMP regulates bacterial persistence through repression
879 of the oxidative stress response and SOS-dependent DNA repair in uropathogenic
880 Escherichia coli. *mBio* **9**, 10–1128 (2018).
881 61. Sulaiman, J. E. & Lam, H. Proteomic investigation of tolerant Escherichia coli populations
882 from cyclic antibiotic treatment. *J Proteome Res* **19**, 900–913 (2020).

883 62. Yamasaki, R., Song, S., Benedik, M. J. & Wood, T. K. Persister cells resuscitate using
884 membrane sensors that activate chemotaxis, lower cAMP levels, and revive ribosomes.
885 *iScience* **23**, (2020).
886 63. Kaldalu, N. & Tenson, T. Slow growth causes bacterial persistence. *Sci Signal* **12**, (2019).
887 64. Wang, Y. *et al.* Inactivation of TCA cycle enhances Staphylococcus aureus persister cell
888 formation in stationary phase. *Sci Rep* **8**, 10849 (2018).
889 65. Zalis, E. A. *et al.* Stochastic Variation in Expression of the Tricarboxylic Acid Cycle
890 Produces Persister Cells. *mBio* **10**, (2019).
891 66. Kim, J.-S. *et al.* Fumarate-Mediated Persistence of Escherichia coli against Antibiotics.
892 *Antimicrob Agents Chemother* **60**, 2232–2240 (2016).
893 67. Spoering, A. L., Vulić, M. & Lewis, K. GlpD and PlsB Participate in Persister Cell Formation
894 in *Escherichia coli*. *J Bacteriol* **188**, 5136–5144 (2006).
895 68. Pandey, S., Sahukhal, G. S. & Elasri, M. O. The msaABCR Operon Regulates Persister
896 Formation by Modulating Energy Metabolism in Staphylococcus aureus. *Front Microbiol*
897 **12**, (2021).
898 69. Shiraliyev, R. C. & Orman, M. Metabolic disruption impairs ribosomal protein levels,
899 resulting in enhanced aminoglycoside tolerance. *bioRxiv* 2012–2023 (2023).
900 70. Datsenko, K. A. & Wanner, B. L. One-step inactivation of chromosomal genes in
901 *Escherichia coli* K-12 using PCR products. *Proceedings of the National Academy of*
902 *Sciences* **97**, 6640–6645 (2000).
903 71. Tirabassi, R. & Bio, B. Foundations of Molecular Cloning-Past, Present and Future. *NEB,*
904 *New England Bio Labs Inc, www. neb. com/tools-and-*
905 *resources/featurearticles/foundations-of-molecular-cloning-past-present-and-future*
906 (2014).
907 72. Amato, S. M., Orman, M. A. & Brynildsen, M. P. Metabolic Control of Persister Formation
908 in Escherichia coli. *Mol Cell* **50**, 475–487 (2013).
909 73. De Groote, V. N. *et al.* Novel persistence genes in *Pseudomonas aeruginosa* identified by
910 high-throughput screening. *FEMS Microbiol Lett* **297**, 73–79 (2009).
911 74. Keren, I., Shah, D., Spoering, A., Kaldalu, N. & Lewis, K. Specialized Persister Cells and the
912 Mechanism of Multidrug Tolerance in *Escherichia coli*. *J Bacteriol* **186**, 8172–8180 (2004).
913 75. Mohiuddin, S. G., Nguyen, T. V. & Orman, M. A. Pleiotropic actions of phenothiazine
914 drugs are detrimental to Gram-negative bacterial persister cells. *Commun Biol* **5**, 217
915 (2022).
916 76. Aguilan, J. T., Kulej, K. & Sidoli, S. Guide for protein fold change and *p* -value calculation
917 for non-experts in proteomics. *Mol Omics* **16**, 573–582 (2020).
918 77. Mohiuddin, S. G., Hoang, T., Saba, A., Karki, P. & Orman, M. A. Identifying Metabolic
919 Inhibitors to Reduce Bacterial Persistence. *Front Microbiol* **11**, (2020).
920 78. YUEN, K. K. The two-sample trimmed *t* for unequal population variances. *Biometrika* **61**,
921 165–170 (1974).
922 79. Opalek, M., Smug, B. J. & Wloch-Salamon, D. How to determine microbial lag phase
923 duration? *bioRxiv* 2011–2022 (2022).
924

925 **Figure Legends**

**Figure 1: Crp/cAMP Regulation of Persister Cell Formation in the Stationary Phase.** *E. coli* K-12 MG1655 WT and mutant cells at early (t=5h) and late (t=24h) stationary phases were transferred to fresh medium with antibiotics for persister cell quantification. At time points 0, 2, 6, 8, and 20h, 1 mL of the treated culture underwent two washes with 1X phosphate-buffered saline (PBS) to remove antibiotics. It was then serially diluted and plated on an agar plate to count the colony-forming units (CFUs). **(a)** Persister levels of ampicillin-treated culture with an antibiotic concentration of 200 µg/mL. **(b)** Persister levels of ofloxacin-treated culture with an antibiotic concentration of 5 µg/mL. **(c)** Persister levels of gentamicin-treated culture with an antibiotic concentration of 50 µg/mL. The number of biological replicates is n=4 for all panels. Biphasic kill curves were generated using a non-linear model (see Materials and Methods). Statistical significance tests were conducted using F-statistics (*$P < 0.05$, **$P < 0.01$, ****$P < 0.0001$). The data for each time point represent the mean value ± standard deviation.

**Figure 2: The effect of Crp/cAMP on Persister Cell Metabolism during Stationary Phase. (a)** MS analysis of *E. coli* K-12 MG1655 WT, Δ*crp*, and Δ*cyaA* at early (t=5h) and late (t=24h) stationary phases. Unsupervised hierarchical clustering was applied to standardized metabolic data. Each column represents a biological replicate. n=4. **(b)** Pathway enrichment analysis was conducted using MetaboAnalyst[47]. Upregulated and downregulated pathways of the Δ*crp* strain compared to WT in the late-stationary growth phase were provided in this figure (refer to Supplementary Fig. 5, 6, and 7 for the other pairwise comparisons). **(c, d)** Pathway enrichment maps comparing metabolites of the TCA cycle, pentose phosphate metabolism, glycolysis, gluconeogenesis, and pyruvate metabolism in Δ*crp* versus WT for ESP and LSP conditions, respectively. Circle size corresponds to the ratio of normalized metabolite intensities between mutant and control cells. Blue ($P \leq 0.05$ for dark blue; $0.05 < P < 0.10$ for light blue) and red ($P \leq 0.05$ for dark red; $0.05 < P < 0.10$ for light red) indicate significantly downregulated or upregulated metabolites in the mutant compared to the control. White signifies no significant difference. n=4 for all panels. ESP: Early stationary phase, LSP: Late stationary phase.

**Figure 3: Validation of Crp/cAMP-Mediated Metabolic State in Persister Cells Through Proteomics Analysis.** Pathway enrichment analysis was conducted in STRING [48,49] for upregulated **(panel a)** and downregulated **(panel b)** proteins. Genes highlighted in red are linked with the upregulated protein networks, while genes in blue, gray, and purple correspond to those in the downregulated protein network. The visual network in STRING illustrates protein interactions. In evidence mode, color in the network represents the interaction evidence of data support, derived from curated databases, experimental data, gene neighborhood, gene fusions, co-occurrence, co-expression, protein homology, and text mining [48,49].

**Figure 4: The Role of Crp/cAMP in Non-Growing Cell Formation. (a, b)** Flow cytometry histograms depict mCherry expression in *E. coli* K-12 MG1655 WT, Δ*crp*, and Δ*cyaA* at early (t=5h) and late (t=24h) stationary phases, respectively. Cells containing an IPTG-inducible mCherry expression system were cultivated with IPTG. After washing and dilution of early and late stationary phase cells in IPTG-free fresh media, fluorescence was tracked in non-growing and growing cells for 2.5 hours. The panel is a representative biological replicate. Consistent results were seen across all 3 biological replicates. **(c)** Growth curves of WT, Δ*crp*, and Δ*cyaA* cultures were determined using flow cytometry to calculate lag and doubling times. Lag times

969 were calculated using the "Microbial lag phase duration calculator" [79]. Doubling times were
970 computed using the formula $t_d=\Delta t/(3.3xLog_{10}(N/N_o))$. n=3. *Statistical significance observed
971 between control and mutant strains (P < 0.05, 2-tailed t-test). The data for each time point
972 represent the mean value ± standard deviation.

973 **Figure 5: Crp/cAMP-Mediated Metabolic State of Persister Cells. (a)** GFP reporter plasmid
974 introduced into *E. coli* K-12 MG1655 WT, Δ*crp*, and Δ*cyaA* cells to monitor SQR gene activity.
975 Flow cytometry was used to detect activity at early (t=5h) and late (t=24h) stationary phases.
976 The panel on the left represents a biological replicate, and the results are consistent across all 3
977 replicates, as demonstrated in the panel on the right. Statistical significance observed between
978 control and mutant groups (*P < 0.05, **P < 0.01, ***P < 0.001, 2-tailed t-test). **(b)** Redox
979 activities of *E. coli* K-12 MG1655 WT, Δ*crp*, and Δ*cyaA* cells were measured at early (t=5h) and
980 late (t=24h) stationary phases by flow cytometry using a RSG dye. This dye fluoresces green
981 after reduction by bacterial reductases. A representative biological replicate is shown (left),
982 with consistent results across all 5 replicates (right). Statistical significance observed between
983 control and mutant groups (*P < 0.05, **P < 0.01, 2-tailed t-test). **(c)** *E. coli* cells with integrated
984 mCherry expression system used to validate cellular respiration. Cells were diluted into fresh
985 media and treated with ampicillin (200 µg/mL) for 20 hours. Flow cytometry measured the red
986 fluorescence of intact surviving cells. A representative biological replicate is shown, with
987 consistent results across all 3 replicates. **(d)** RSG levels of cells (carrying the mCherry expression
988 system) at exponential phase (t=3h); cells before ampicillin treatment; non-lysed (intact) cells
989 after 20 hours of ampicillin treatment; and untreated cells after 20 hours of culturing. A
990 representative biological replicate is shown (left), with consistent results across all 4 replicates
991 (right). Statistical significance observed between intact antibiotic-treated cells and others (*P <
992 0.05, **P < 0.01, 2-tailed t-test). **(e)** High throughput screening of mutants from Keio collection.
993 The mutant strains selected are associated with central metabolism. Stationary phase cells
994 were diluted 100-fold in fresh medium and treated with ampicillin (200 µg/mL) or ofloxacin (5
995 µg/mL) for 20 hours. Treated cultures were washed, serially diluted, and plated on agar plates
996 to quantify CFUs. **(f)** Genes related to the TCA cycle, ETC, ATP synthase, glycolysis, and pentose
997 phosphate pathway (PPP) were knocked out and then treated with ampicillin (200 µg/mL) or
998 ofloxacin (5 µg/mL) to enumerate CFUs. n=4. Biphasic kill curves were generated using a non-
999 linear model. Statistical significance tests were conducted using F-statistics (*P < 0.05, and
1000 **P < 0.01). Each data point represents the mean value ± standard deviation.

1001

1002

1003

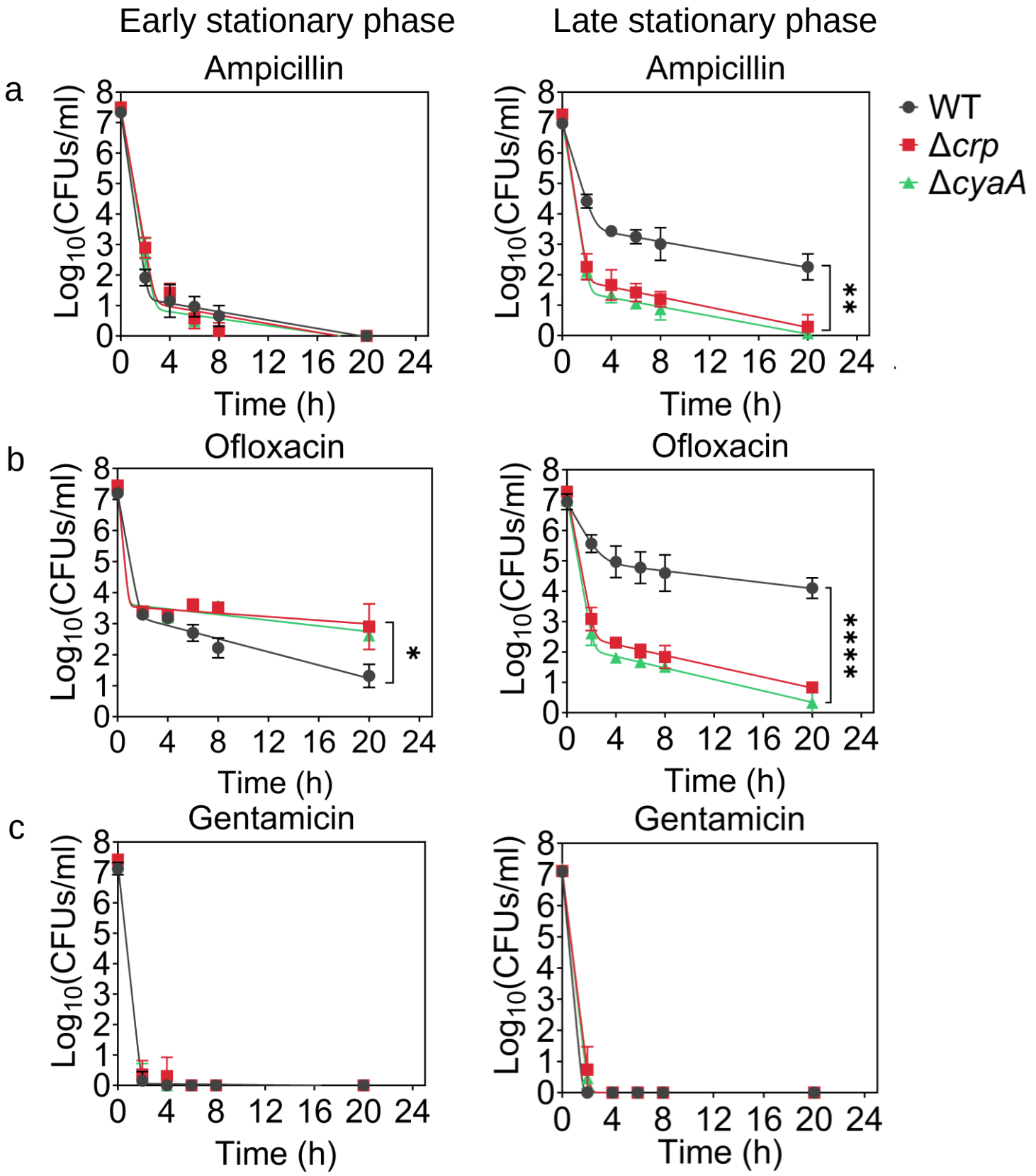
Early stationary phase
Late stationary phase
a
Ampicillin
Ampicillin
b
Ofloxacin
Ofloxacin
c
Gentamicin
Gentamicin
Log10(CFUs/ml)
Time (h)
WT
Δcrp
ΔcyaA
*
**
***

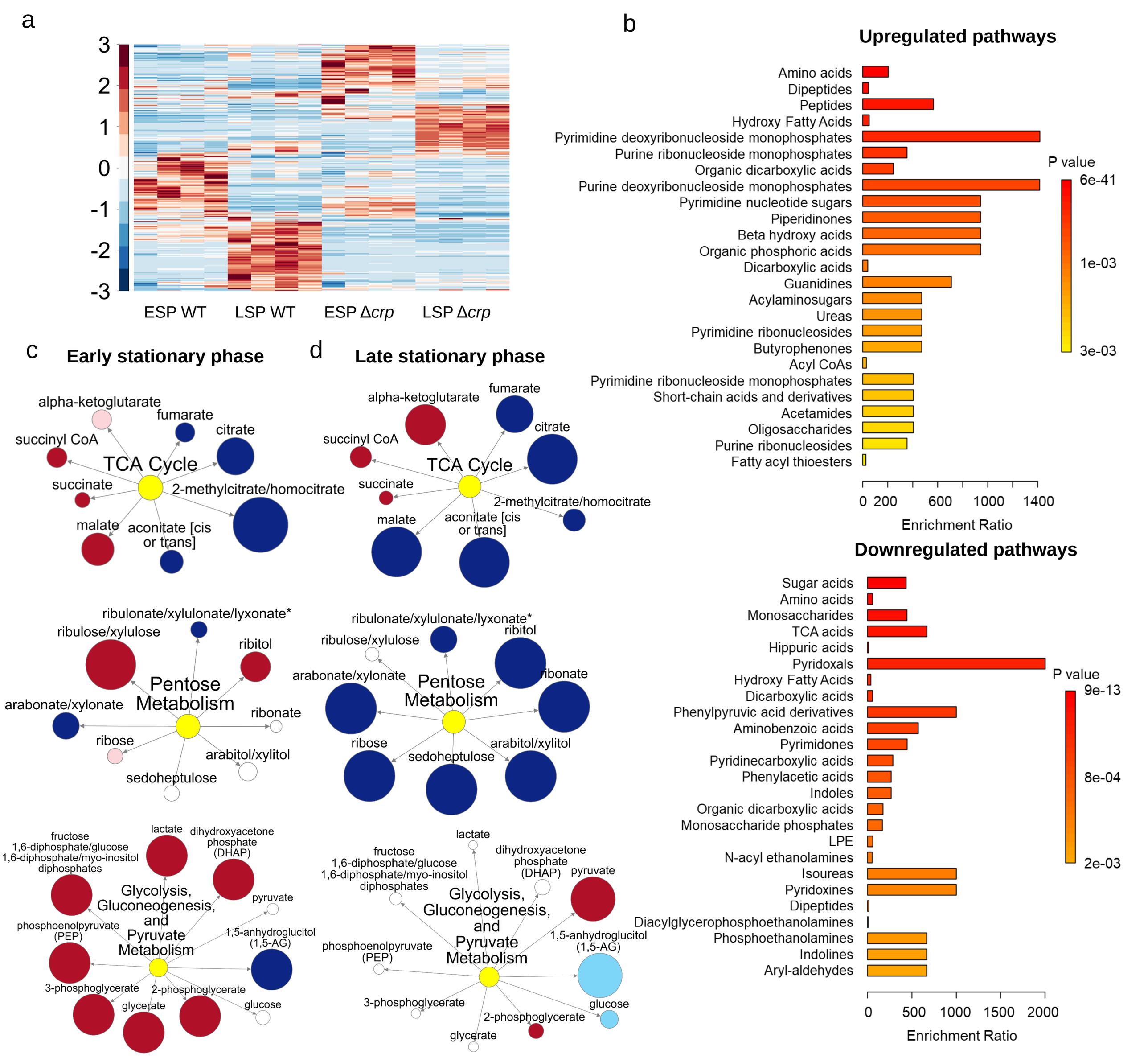


**Upregulated (red circle) and downregulated (blue circle) metabolites in the Δ*crp* strain compared to WT**

a

## Upregulated pathways

- Anabolic metabolism
- Peptidoglycan metabolic processes
- Cell wall organization or biogenesis
- Cellular component organization or biogenesis
- Regulation of cell shape, cell cycle, and cell division

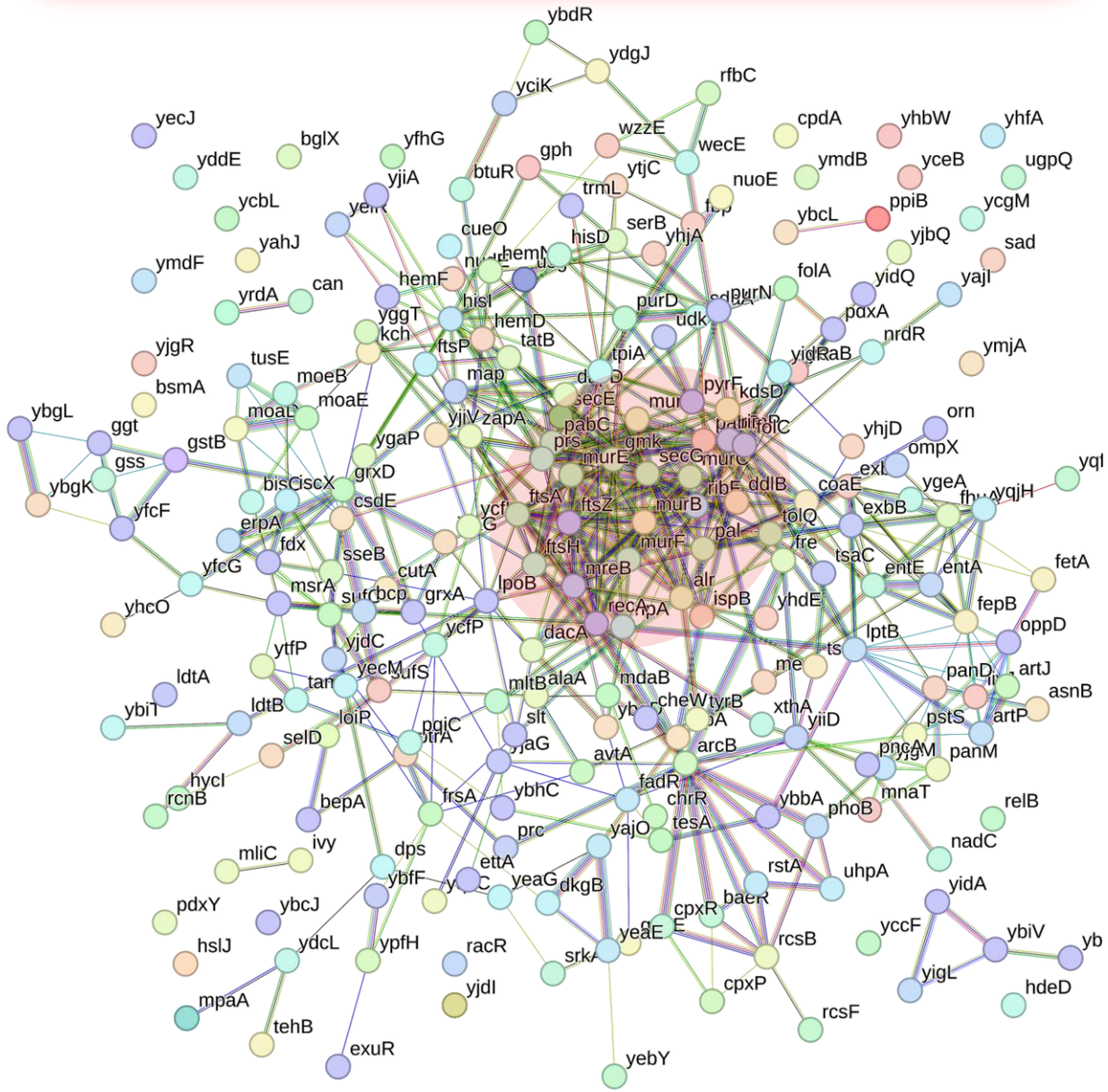

b

## Downregulated pathways

- Ribosome and translation factor activity
- Translation, and protein export
- Ribonucleoprotein, and translation factor activity
- RNA binding

- Tricarboxylic acid cycle
- Glycerol metabolism
- Pyruvate metabolism
- Glycolysis
- Energy metabolism
- Respiratory processes

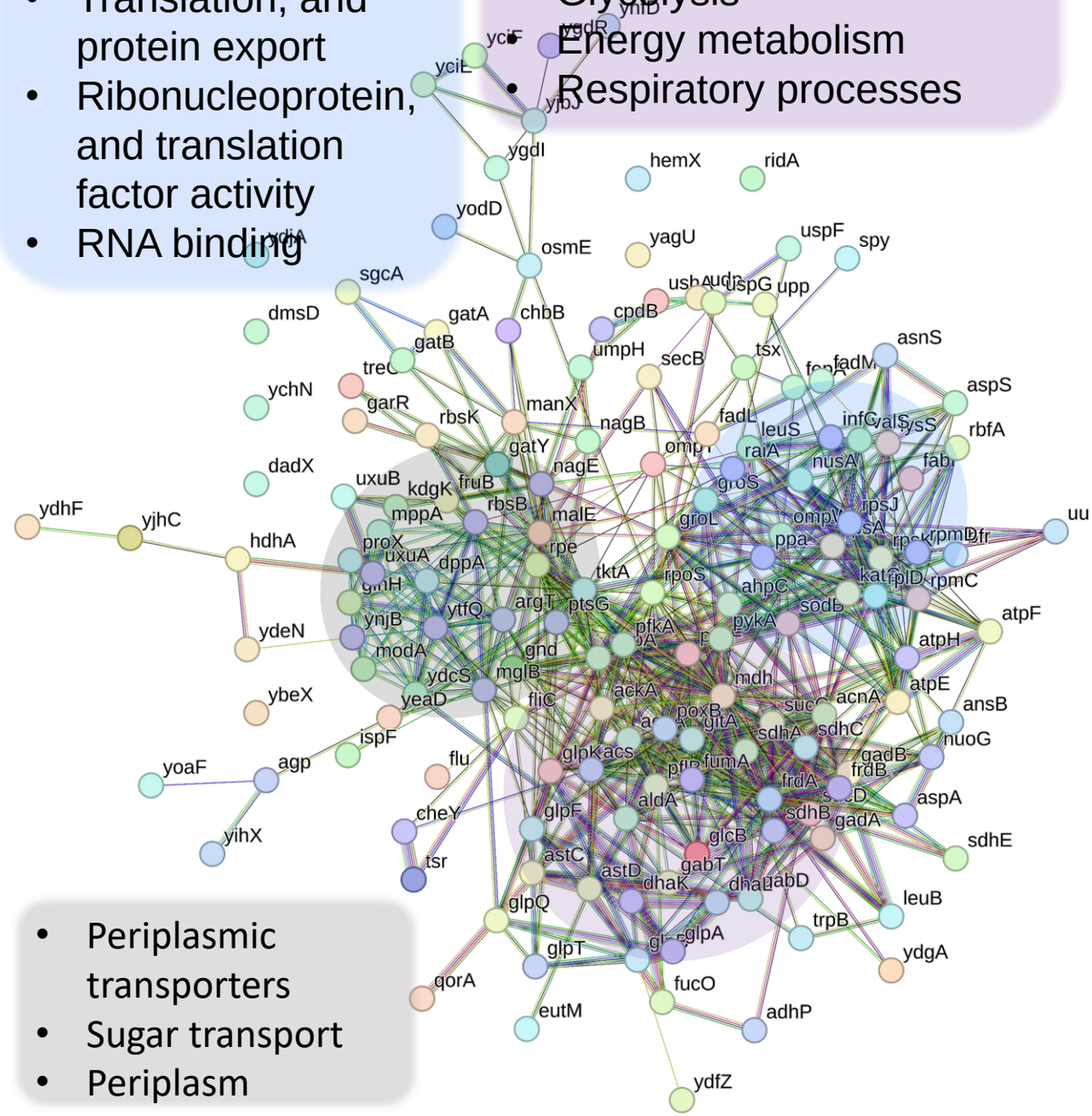

- Periplasmic transporters
- Sugar transport
- Periplasm

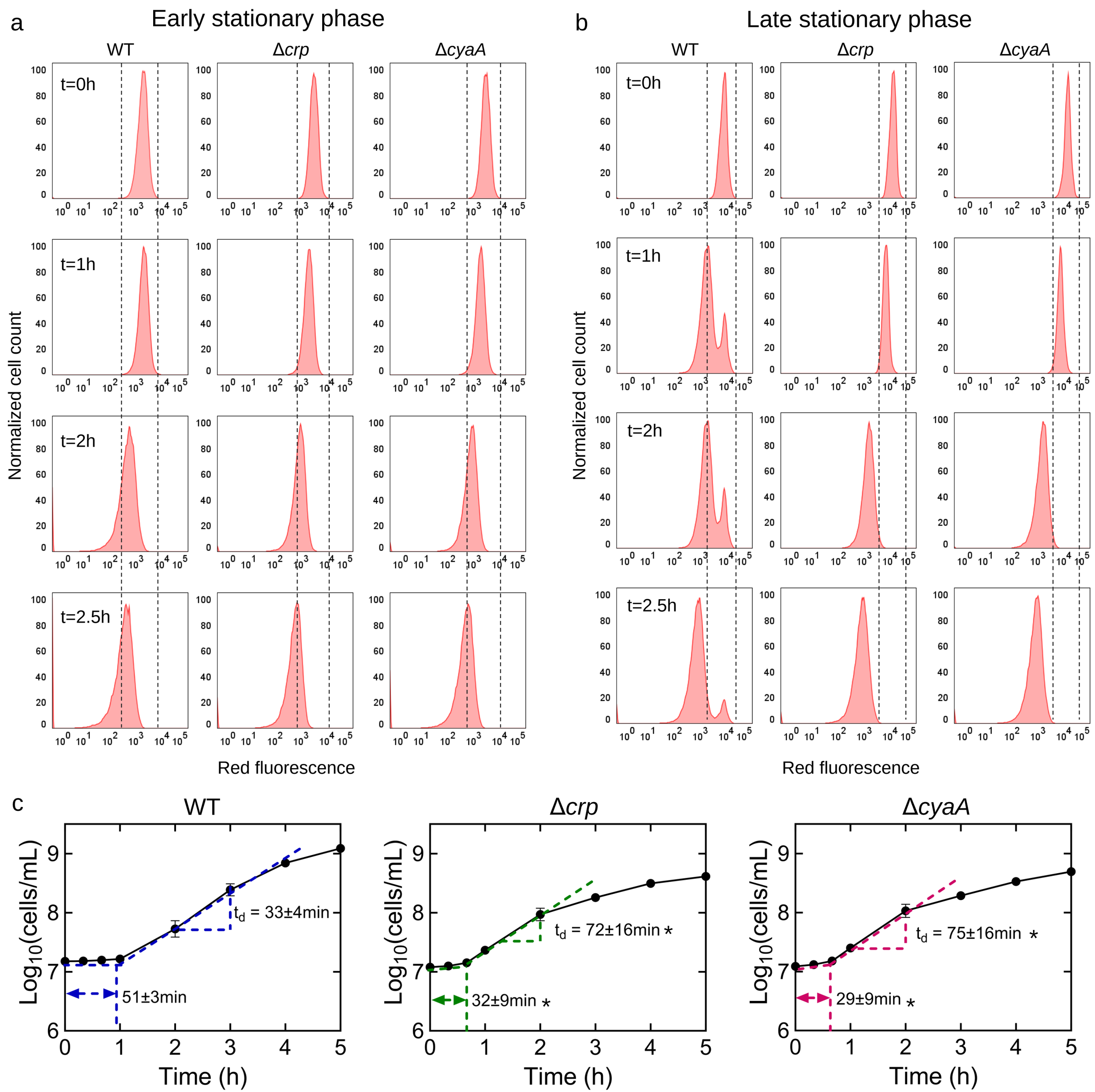
a
Early stationary phase
WT
Δcrp
ΔcyaA
t=0h
t=1h
t=2h
t=2.5h
Normalized cell count
Red fluorescence
b
Late stationary phase
WT
Δcrp
ΔcyaA
t=0h
t=1h
t=2h
t=2.5h
Normalized cell count
Red fluorescence
c
WT
Δcrp
ΔcyaA
Log10(cells/mL)
Time (h)
td = 33±4min
51±3min
td = 72±16min *
32±9min *
td = 75±16min *
29±9min *

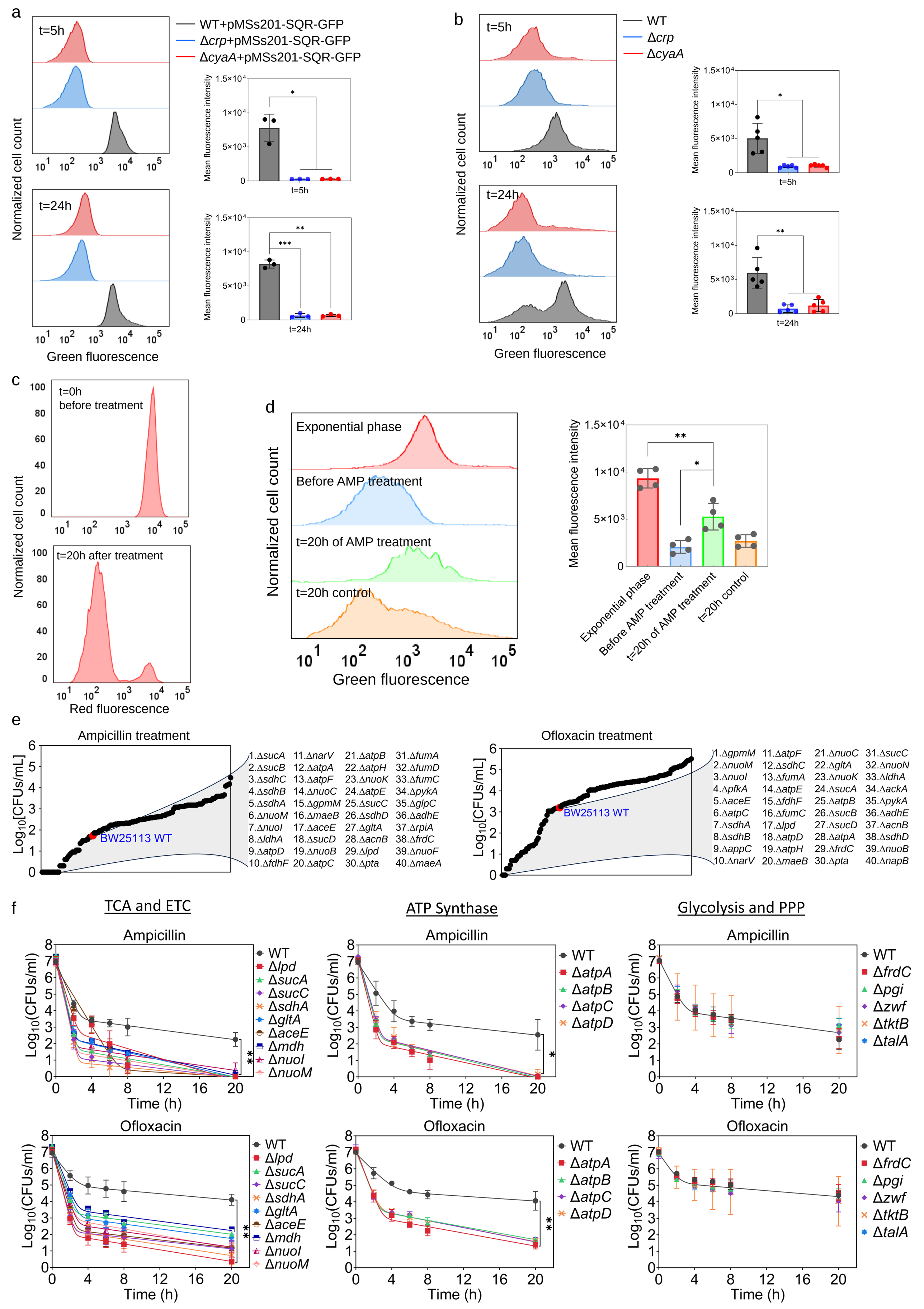
a
t=5h
t=24h
WT+pMSs201-SQR-GFP
Δcrp+pMSs201-SQR-GFP
ΔcyaA+pMSs201-SQR-GFP
Normalized cell count
Green fluorescence
Mean fluorescence intensity
b
WT
Δcrp
ΔcyaA
c
t=0h
before treatment
t=20h after treatment
Red fluorescence
d
Exponential phase
Before AMP treatment
t=20h of AMP treatment
t=20h control
e
Ampicillin treatment
Ofloxacin treatment
BW25113 WT
Log10[CFUs/mL]
1.ΔsucA 2.ΔsucB 3.ΔsdhC 4.ΔsdhB 5.ΔsdhA 6.ΔnuoM 7.ΔnuoI 8.ΔldhA 9.ΔatpD 10.ΔfdhF 11.ΔnarV 12.ΔatpA 13.ΔatpF 14.ΔnuoC 15.ΔgpmM 16.ΔmaeB 17.ΔaceE 18.ΔsucD 19.ΔnuoB 20.ΔatpC 21.ΔatpB 22.ΔatpH 23.ΔnuoK 24.ΔatpE 25.ΔsucC 26.ΔsdhD 27.ΔgltA 28.ΔacnB 29.Δlpd 30.Δpta 31.ΔfumA 32.ΔfumD 33.ΔfumC 34.ΔpykA 35.ΔglpC 36.ΔadhE 37.ΔrpiA 38.ΔfrdC 39.ΔnuoF 40.ΔmaeA
1.ΔgpmM 2.ΔnuoM 3.ΔnuoI 4.ΔpfkA 5.ΔaceE 6.ΔatpC 7.ΔsdhA 8.ΔsdhB 9.ΔappC 10.ΔnarV 11.ΔatpF 12.ΔsdhC 13.ΔfumA 14.ΔatpE 15.ΔfdhF 16.ΔfumC 17.Δlpd 18.ΔatpD 19.ΔatpH 20.ΔmaeB 21.ΔnuoC 22.ΔgltA 23.ΔnuoK 24.ΔsucA 25.ΔatpB 26.ΔsucB 27.ΔsucD 28.ΔatpA 29.ΔfrdC 30.Δpta 31.ΔsucC 32.ΔnuoN 33.ΔldhA 34.ΔackA 35.ΔpykA 36.ΔadhE 37.ΔacnB 38.ΔsdhD 39.ΔnuoB 40.ΔnapB
f
TCA and ETC
ATP Synthase
Glycolysis and PPP
Ampicillin
Ofloxacin
Log10(CFUs/ml)
Time (h)
WT
Δlpd
ΔsucA
ΔsucC
ΔsdhA
ΔgltA
ΔaceE
Δmdh
ΔnuoI
ΔnuoM
ΔatpA
ΔatpB
ΔatpC
ΔatpD
ΔfrdC
Δpgi
Δzwf
ΔtktB
ΔtalA